RESEARCH ARTICLES

Phosphorylated transcription factor PuHB40 is involved in ROS-dependent anthocyanin biosynthesis in pear exposed to high-light stress

Lu Zhang[1], Lu Wang[1], Yongchen Fang[1], Yuhao Gao[1], Shulin Yang[1], Jun Su[2], Junbei Ni[1], Yuanwen Teng[1,3] & Songling Bai[1,*]

[1]College of Agriculture and Biotechnology, Zhejiang University, Hangzhou 310058, Zhejiang, China

[2]Institute of Horticulture, Yunnan Academy of Agricultural Sciences, Kunming 650205, China

[3]Hainan Institute of Zhejiang University, Sanya, Hainan 572000, China.

Short title: PuHB40 promotes ROS-dependent anthocyanin biosynthesis

*Corresponding author: Songling Bai (songlingbai@zju.edu.cn)

The author responsible for distribution of materials integral to the findings presented in this article in accordance with the policy described in the Instructions for Authors (https://academic.oup.com/plcell/pages/General-Instructions) is: Songling Bai (songlingbai@zju.edu.cn).

ABSTRACT

As sessile organisms, plants are increasingly vulnerable to environmental stresses because of global warming and climate change. Stress-induced reactive oxygen species (ROS) accumulation results in plant cell damages and even cell death. Anthocyanins are important antioxidants that scavenge ROS to maintain ROS homeostasis. However, the mechanism underlying ROS-induced anthocyanin accumulation is unclear. In this study, we determined that in pear the HD-Zip I family member PuHB40 mediates ROS-dependent anthocyanin biosynthesis under high-light stress. Specifically, PuHB40 is a transcription factor that induces PuMYB123-like/PubHLH3 complex for anthocyanin biosynthesis. The transcriptional activation by PuHB40 depends on its phosphorylation level, which is regulated by protein phosphatase 2A (PP2A). High ROS contents maintain the phosphorylation of PuHB40 at a high level, while also enhancing PuHB40-induced *PuMYB123-like* transcription by decreasing the transcription of *PuPP2AA2*, ultimately leading to increased anthocyanin biosynthesis. Our study revealed the pathway regulating ROS-induced anthocyanin biosynthesis in pear, further clarifying the mechanism underlying abiotic stress-induced anthocyanin biosynthesis, which may have implications for improving plant stress tolerance.

Keywords: high-light stress, ROS, anthocyanin biosynthesis, PuHB40, PuMYB123-like, PP2A phosphatase, dephosphorylation

44 **IN A NUTSHELL**

45 **Background:** Various abiotic stresses, including high-light intensity, promote the
46 accumulation of anthocyanins in plants, while also activating the production of reactive
47 oxygen species (ROS). Anthocyanins can attenuate the negative effects of high-light stress
48 by acting as antioxidants that restrict ROS accumulation. Several reports have shown that
49 ROS can stimulate anthocyanin accumulation, but whether high-light stress-induced
50 anthocyanin accumulation depends on ROS is undetermined. Additionally, the mechanism
51 underlying ROS-dependent anthocyanin biosynthesis remains unclear.

52 **Question:** Does high-light stress-induced anthocyanin biosynthesis depend on ROS? What
53 is the molecular basis of high-light stress-induced anthocyanin biosynthesis?

54 **Findings:** High-light stress-induced anthocyanin biosynthesis in pear seedlings is
55 dependent on ROS accumulation. PuMYB123-like is the key MYB transcription factor for
56 anthocyanin biosynthesis, while PuHB40 activates anthocyanin biosynthesis in response
57 to ROS under high-light stress. Specifically, PuHB40 activates the transcription of
58 *PuMYB123-like*, with the encoded protein combining with PubHLH3 to form an MBW
59 complex that promotes anthocyanin biosynthesis. The transcriptional activation by
60 PuHB40 depends on its phosphorylation status, which is regulated by protein phosphatase
61 2A (PP2A). High ROS levels inhibit the transcription of *PuPP2AA2*, thereby maintaining
62 the phosphorylation of PuHB40, enhancing the transcriptional activation by PuHB40,
63 inducing *PuMYB123-like* transcription, and ultimately leading to increased anthocyanin

64 biosynthesis.

65 **Next steps:** Our future research will focus on whether ROS and the MYB123-like–
66 PuHB40–PP2A regulatory module are also involved in the anthocyanin biosynthesis
67 induced by other abiotic and biotic stresses, which will provide insights into biotic stress-
68 induced anthocyanin biosynthesis and form the theoretical basis for improving fruit
69 coloration.

70

71 **INTRODUCTION**

72 Because of global warming and climate change, plants are increasingly becoming more
73 susceptible to a variety of environmental stresses (e.g., drought, salinity, cold, and high-
74 light) during growth and development, which leads to changes in physiological and
75 biochemical metabolism, including the dramatic accumulation of reactive oxygen species
76 (ROS) (Hipsch et al. 2021; Mittler et al. 2022). Light is one of the most indispensable
77 environmental factors for plants. It provides energy for photosynthesis, which converts
78 carbon dioxide (CO_2) and water into energy-rich organic matter required for plant
79 physiological metabolism (Croce and van Amerongen 2014). Under high-light stress
80 conditions, photon flux exceeds the energy needed by plants to fix CO_2, with O_2^- and $_1O^2$
81 primarily produced in chloroplasts by photosystems I and II, respectively, while H_2O_2 is
82 generated in peroxisomes if photorespiration is activated (Galvez-Valdivieso et al. 2009;
83 Kerchev et al. 2016; Wang et al. 2020; Mittler et al. 2022). Excessive ROS accumulation
84 adversely affects the surrounding biological system components, including membranes,

85 proteins, and DNA, and then triggers physiological processes that lead to programmed cell
86 death (Lee and Gould 2002; Mittler 2017). Anthocyanins are important specialized
87 metabolites that can function as non-enzymatic antioxidants that maintain ROS
88 homeostasis and limit the damage due to stress-induced ROS. Moreover, their antioxidant
89 capacity is greater than that of other flavonoids or even ascorbic acid and vitamin E (Gould
90 et al. 2002; Bi et al. 2014; Acero et al. 2019). Considering various abiotic stresses promote
91 anthocyanin accumulation in plants (Catalá et al. 2011; Xie et al. 2012; Jaakola 2013;
92 Nakabayashi et al. 2014) and ROS can induce anthocyanin production (Xu et al. 2017; Shi
93 et al. 2018), ROS may influence abiotic stress-induced anthocyanin biosynthesis; this
94 hypothesis has been tested in a few studies (Wu et al. 2016; Qu et al. 2018; Shi et al. 2022).
95 Anthocyanins are synthesized in the phenylpropanoid pathway by various enzymes
96 encoded by structural genes. Examples include phenylalanine ammonia-lyase (PAL),
97 chalcone synthase (CHS), chalcone isomerase (CHI), flavanone 3-hydroxylase (F3H),
98 flavonoid 3′-hydroxylase (F3′H), dihydroflavonol 4-reductase (DFR), anthocyanin
99 synthase (ANS), and UDP-glucose: flavonoid 3-glucosyltransferase (UFGT) (Xu et al.
100 2015; Liu et al. 2021; Pratyusha and Sarada 2022). The R2R3-MYB and basic helix–loop–
101 helix (bHLH) transcription factors (TFs) combine with WD-repeat proteins to form MBW
102 complexes in which MYBs function as major regulators of structural gene expression
103 (Jaakola 2013; Xu et al. 2015; Naing and Kim 2018). The R2R3-MYB TFs are divided into
104 25 subgroups, among which subgroup 6 contains TFs that are mainly responsible for

105 promoting anthocyanin biosynthesis, including PAP1 (AtMYB75), PAP2 (AtMYB90), and
106 AtMYB113 in *Arabidopsis thaliana* (Dubos et al. 2010) as well as PpMYB10 and
107 PpMYB114 in pear (Feng et al. 2010; Yao et al. 2017). The expression of MYB TFs is
108 regulated by various factors, including light (Takos et al. 2006; Li et al. 2012; Bai et al.
109 2019a), low/high temperatures (Choi et al. 2009; Lin-Wang et al. 2011; Xie et al. 2012),
110 and phytohormones (Shan et al. 2009; Das et al. 2012; Ni et al. 2023). The encoded MYB
111 TFs control the expression of anthocyanin biosynthetic structural genes. To date, the
112 molecular basis of ROS-induced anthocyanin biosynthesis remains relatively
113 uncharacterized.

114 In cells, the accumulation of ROS alters the redox state and the post-translational
115 modification of proteins, especially the phosphorylation of proteins. ROS signal is
116 transduced by Ca^{2+}, Ca^{2+} binding protein, phosphatidic acid (PA) and phospholipase D
117 (PLD) and activates OXIDATIVE SIGNAL-INDUCIBLE 1 (OXI1), which subsequently
118 activates MAPK cascade pathway, which in turn promotes the phosphorylation of
119 downstream transcription factors, such as WRKY proteins and AP2/ethylene-response
120 factors (ERFs) (Kovtun et al. 2000; Jalmi and Sinha 2015; Byrne et al. 2020; Mittler et al.
121 2022). Furthermore, the phosphorylation of transcription factors are also regulated by
122 phosphatase, such as PTP1 (protein tyrosine phosphatase 1), SAL1 (3'-phosphoadenosine
123 5'-phosphate phosphatase) and PP2C, whose activity are regulated by ROS levels (Gupta
124 and Luan 2003), oxidative stresses (Chan et al. 2016) or phytohormones (Mine et al. 2017).

125 The PP2A holoenzyme, which is a serine/threonine-specific phosphatase, is a
126 heterotrimeric complex comprising a catalytic subunit C, a regulatory subunit B, and a
127 structural subunit A. The A subunit has a conserved structure consisting of 15 tandem
128 repeats of a 39 amino acid sequence (i.e., HEAT motif) (Janssens and Goris 2001). In *A.*
129 *thaliana*, three A subunits of PP2A have been identified, namely PP2AA1 (RCN1),
130 PP2AA2, and PP2AA3. The phosphatase activity of PP2A plays an important role in stress
131 response (DeLong 2006; Uhrig et al. 2013; Lillo et al. 2014; Durian et al. 2016). However,
132 it is not clear whether PP2A phosphatases are involved in ROS regulation of protein
133 phosphorylation under stress conditions.

134 In this study, we determined that abiotic stress-induced anthocyanin biosynthesis is at
135 least partially dependent on ROS in pear. The HD-Zip I family member PuHB40 was
136 identified as the key TF involved in ROS-dependent anthocyanin biosynthesis. Notably,
137 PuHB40 functions as the upstream positive regulator of the PuMYB123-like/PubHLH3
138 complex during anthocyanin biosynthesis. The dephosphorylation of PuHB40, which is
139 catalyzed by protein phosphatase 2A (PP2A), inhibits its function related to ROS-induced
140 anthocyanin biosynthesis. Under abiotic stress conditions, ROS inhibit the transcription of
141 *PuPP2AA2*. This study revealed the pathway regulating ROS-induced anthocyanin
142 biosynthesis in pear under high-light stress, providing important insights into the
143 mechanism mediating abiotic stress-induced anthocyanin production.

144 **RESULTS**

145 **Stress induced ROS promoted anthocyanin biosynthesis in pear seedlings**

146 To test whether abiotic stress-induced anthocyanin biosynthesis depends on ROS
147 production, pear seedlings (*P. ussuriensis*) grown under continuous light were exposed to
148 abiotic stresses, including salt, drought, and high-light, and the N,N′-dimethylthiourea
149 (DMTU) was used to decrease the ROS content under abiotic stress conditions. DMTU is
150 a highly permeant molecule that can scavenge hydrogen peroxide (H_2O_2), the hydroxyl
151 radical (·OH), or hypochlorous acid (HOCl) *in vitro* (Curtis et al. 1988; Serobatse and
152 Kabanda 2017). It has been widely used to remove ROS in plant studies (Ni et al. 2019;
153 Deng et al. 2022). The various abiotic stresses caused anthocyanins to accumulate in pear
154 seedlings after seven days, but anthocyanin production decreased significantly following
155 the DMTU treatment (Supplemental Fig. S1A), indicating that ROS are potentially
156 involved in stress-induced anthocyanin production. Furthermore, ROS accumulation and
157 anthocyanin biosynthesis were examined at 0, 6, 12, 24, 48, 72, and 96 h after plants
158 underwent the high-light treatment (Fig. 1A). Anthocyanin accumulation peaked at the 72-
159 h time-point and then decreased, but this accumulation was significantly suppressed in the
160 seedlings that were also treated with DMTU (Fig. 1B). The NBT and DAB staining results
161 indicated that DMTU suppressed the accumulation of O_2^- and H_2O_2 in pear leaves exposed
162 to high-light stress (Fig. 1C–F). These findings were supported by the analysis of H_2O_2
163 contents (Fig. 1G). Moreover, in response to the different stress treatments (e.g. high-light
164 stress, drought stress, and salt stress), the anthocyanin and H_2O_2 contents accumulated in

165 the same leaf regions (Supplemental Fig. S1B). According to these results, abiotic stress-
166 induced anthocyanin accumulation depends on ROS production. Hence, the ROS
167 scavenger DMTU can inhibit ROS accumulation and indirectly decrease anthocyanin
168 production.

169 To identify the key genes responsible for abiotic stress-induced anthocyanin
170 biosynthesis, the expression of anthocyanin-related structural and regulatory genes was
171 analyzed. The *PuCHI*, *PuCHS*, *PuDFR*, *PuF3H*, and *PuANS* expression levels increased
172 significantly and peaked at 48 h after the high-light treatment, which was in accordance
173 with the changes in anthocyanin accumulation. The expression of these genes was
174 significantly inhibited by DMTU (Fig. 1, H-L). In addition, the expression levels of high-
175 light-responsive genes (*PuELIP1* and *PuELIP2*) were significantly upregulated following
176 the high-light treatment with and without DMTU, indicative of the effects of high-light
177 stress (Supplemental Fig. S1C and D). Interestingly, *PuMYB10*, which encodes a critical
178 TF that regulates light-induced anthocyanin biosynthesis in pears, was similarly expressed
179 following the high-light stress and DMTU treatments (Fig. 1M), even though these two
180 treatments resulted in significant differences in anthocyanin accumulation and the
181 expression of downstream structural genes. These findings suggest that other TFs may be
182 involved in regulating ROS-dependent anthocyanin biosynthesis.

183 **Identification of PuMYB123-like and its interaction with PubHLH3**

184 To determine which TFs participate in ROS-dependent anthocyanin biosynthesis, the high-

185 light stress- and DMTU-treated pear seedlings underwent an RNA-seq analysis. A
186 weighted gene co-expression network analysis was conducted using the fragments per
187 kilobase of transcript per million reads mapped (FPKM) values of anthocyanin-related
188 structural genes (*PuCHS*, *PuCHI*, *PuF3H*, *PuDFR*, and *PuANS*) as trait data for identifying
189 genes that are co-expressed with anthocyanin biosynthetic genes. A total of 23 modules
190 were identified, with the "purple" module most highly correlated with the trait data
191 (Supplemental Fig. S2). The "purple" module included nine MYB TF genes, of which eight
192 encoded R2R3-MYB TFs (Supplemental Data Set S5). Finally, *PuMYB123-like*
193 (EVM0034726.1) was more significantly induced by high-light stress than the other seven
194 R2R3-MYB TF genes (Supplemental Fig. S3). Accordingly, it was selected for further
195 study. The *PuMYB123-like* expression level, which was consistent with that of anthocyanin
196 biosynthesis structural genes, increased rapidly in response to high-light stress and peaked
197 at 48 h, but the DMTU treatment inhibited *PuMYB123-like* expression (Fig. 2A). The
198 multiple sequence alignment showed PuMYB123-like contains a typical R2R3 repeat in
199 the N-terminal, with a bHLH motif in the R3 repeat region that can interact with bHLH
200 TFs (Supplemental Fig. S4B). The subcellular localization analysis showed that the
201 fluorescence of GFP-tagged PuMYB123-like was predominantly distributed in the nucleus,
202 consistent with the characteristics of TFs (Fig. 2C). Considered together, these results
203 indicate that PuMYB123-like is a transcriptional factor that may contribute to ROS-
204 dependent anthocyanin biosynthesis.

205 Considering MYB and bHLH TFs combine with WD-repeat proteins to form MBW
206 complexes that control the expression of anthocyanin-related structural genes, we assessed
207 whether PuMYB123-like can interact with three candidate bHLH TFs (PubHLH3,
208 PubHLH33, and PubHLH64), which affect anthocyanin biosynthesis in pear (Tao et al.
209 2020; Ni et al. 2021). According to the yeast two-hybrid (Y2H) assay results, PuMYB123-
210 like can bind to PubHLH3 (Fig. 2D). The interaction was confirmed in pull-down and
211 luciferase complementation imaging (LCI) assays, which revealed PuMYB123-like can
212 interact with PubHLH3 both *in vivo* and *in vitro* (Fig. 2, E and F). Because of the self-
213 activation of PubHLH33 and PubHLH64, the corresponding genes were fragmented to
214 assess potential interactions. The results showed that PuMYB123-like can weakly interact
215 with PubHLH33 (Supplemental Fig. S5A), and interact with the truncated PubHLH64
216 (encoded by 747–1,086 bp) (Supplemental Fig. S5B). According to the dual-luciferase
217 assay, PuMYB123-like can significantly activate the promoter of the anthocyanin-related
218 structural gene *PuCHS*, whereas it weakly activates the *PuANS*, *PuDFR*, and *PuUFGT*
219 promoters (Fig. 2G). However, PubHLH3 significantly enhanced the activation of the
220 *PuCHS*, *PuDFR*, and *PuANS* promoters by PuMYB123-like, whereas PubHLH33 and
221 PubHLH64 had no significant effect (Fig. 2H; Supplemental Fig. S5C). Based on these
222 observations, we proposed that PuMYB123-like, which belongs to subgroup 5 of the
223 R2R3-MYB family, promotes anthocyanin-related structural genes expression as a
224 component of the MBW complex that also includes PubHLH3.

225 **PuMYB123-like promotes anthocyanin biosynthesis in pears**

226 To confirm PuMYB123-like affects anthocyanin biosynthesis, *PuMYB123-like* was
227 overexpressed in pear calli. After a 3-day exposure to light, the anthocyanin contents and
228 anthocyanin biosynthetic gene expression levels were significantly higher in the calli
229 overexpressing *PuMYB123-like* than in the wild-type calli. In addition, the silencing of
230 *PuMYB123-like* in pear calli via RNA interference (RNAi) inhibited anthocyanin
231 biosynthesis and decreased the expression of anthocyanin biosynthetic genes (Fig. 3A-C).
232 Considering PuMYB123-like belongs to subgroup 5 of the R2R3-MYB family, which
233 reportedly regulates proanthocyanin biosynthesis (Baudry et al. 2004; Dubos et al. 2010),
234 the proanthocyanin contents in *PuMYB123-like*-overexpressing (*PuMYB123-like*-OE) pear
235 calli was also examined. There was no significant difference in the proanthocyanin contents
236 of the wild-type and transgenic pear calli (Supplemental Fig. S6A). Additionally,
237 *PuMYB123-like* was ectopically expressed in *Arabidopsis thaliana* to verify the function
238 of the encoded TF. Compared with the wild-type control, the two independent transgenic
239 lines accumulated more anthocyanin (Fig. 3D-F) and had shorter hypocotyls (Fig. 3G). The
240 expression of the anthocyanin biosynthetic genes *AtCHS*, *AtCHI*, *AtDFR*, *AtF3H*, *AtLODX*,
241 and *AtPAP1* increased significantly in the *PuMYB123-like*-expressing lines (Fig. 3H). To
242 examine whether PuMYB123-like mediates anthocyanin biosynthesis in fruits,
243 *PuMYB123-like* was transiently overexpressed in the peel of 'Zaosu' pear fruits that were
244 bagged in advance. The comparison with the control peels (empty vector) after a 3-day

245 exposure to light indicated the *PuMYB123-like*-OE peels had significantly higher
246 anthocyanin contents (Supplemental Fig. S6, B and C), and the transcription level of
247 anthocyanin biosynthetic gene (i.e., *PpCHS*, *PpDFR*, *PpF3H*, *PpANS*, *PpUFGT*,
248 *PpMYB10*, and *PpMYB114*) (Supplemental Fig. S6D). Similarly, 'Hongzaosu' red pear
249 fruit peels in which *PuMYB123-like* was transiently silenced via virus-induced gene
250 silencing (VIGS) had lower anthocyanin contents and anthocyanin biosynthetic gene
251 transcription levels than the control peels (TRV) (Supplemental Fig. S6, E-G). Considered
252 together, these results demonstrate that PuMYB123-like positively regulates anthocyanin
253 biosynthesis in pear.

254 **Identification of PuHB40 and its response to ROS**

255 To identify the TFs that respond to ROS and regulate *PuMYB123-like* expression under
256 high-light stress conditions, we analyzed our RNA-seq data for the high-light stress- and
257 DMTU-treated pear seedlings. A total of 11,608 differentially expressed transcripts (DETs)
258 were identified by pairwise comparisons of mock, high-light stress, and high-light stress
259 supplemented with DMTU treatments at each time point. The DETs were further
260 categorized into 20 clusters according to their expression patterns using Mfuzz
261 (Supplemental Fig. S7). The DETs in cluster 14 were upregulated under high-light stress
262 conditions, but downregulated by the DMTU treatment, indicating the expression of the
263 corresponding genes may increase in response to high-light stress-induced ROS
264 accumulation (Fig. 4A). In addition, 60 genes that were in both the "purple" module

265 (Supplemental Data Set S5) and cluster 14 (Supplemental Data Set S6) were identified (Fig.
266 4B). The transcription of these genes increased following ROS accumulation. Moreover,
267 they were co-expressed with anthocyanin biosynthetic genes. Hence, we considered them
268 as candidate genes involved in ROS-induced anthocyanin biosynthesis. These genes
269 encoded five types of TFs (MYB, MYB-related, bHLH, HD-Zip, and WRKY). In terms of
270 their transcription levels, *PubHLH3* was most highly correlated with *PuMYB123-like*,
271 followed by *PuHB40* (HD-Zip TF) (Fig. 4C). Because PubHLH3 and PuMYB123-like
272 interact to form an MBW complex that controls anthocyanin biosynthesis, PuHB40 was
273 analyzed further. Notably, four HD-Zip TF-binding sites were detected in the *PuMYB123-*
274 *like* promoter (Fig. 4D), suggesting that PuHB40 is the potential regulator of *PuMYB123-*
275 *like* expression under high-light stress conditions.

276 In response to the high-light treatment, the *PuHB40* expression level gradually
277 increased after 24 h, peaked at 48 h, and then decreased, but the DMTU treatment
278 significantly inhibited *PuHB40* expression (Fig. 4F). Additionally, the PuHB40 content
279 changes in response to ROS were analyzed in an immunoblot involving an affinity-purified
280 anti-PuHB40 polyclonal antibody generated in this study (Supplemental Fig. S8). The
281 immunoblot results showed that the PuHB40 protein content increased significantly after
282 6 h of the high-light treatment, after which it gradually decreased, but was maintained at a
283 relatively high level. In contrast, the PuHB40 protein level remained low after the DMTU
284 treatment (Fig. 4G). Hence, PuHB40 was induced by ROS after the abiotic stress treatment.

285 To explore whether PuHB40 is directly affected by ROS, we treated pear calli with 4 mM
286 H_2O_2, which resulted in a significant increase in anthocyanin biosynthesis (Fig. 4H and I).
287 Moreover, the expression of *PcHB40* as well as the anthocyanin-structural genes *PcCHI*,
288 *PcDFR*, *PcF3H*, and *PcANS* also increased (Fig. 4J). Following the H_2O_2 treatment, the
289 *PcHB40* expression level increased after 3 h (Fig. 4K), suggestive of a direct response to
290 H_2O_2.

291 A phylogenetic analysis showed that PuHB40 is a homolog of AT4G36740.1
292 (ATHB40), while a multiple sequence alignment revealed a conserved homeodomain and
293 leucine zipper in PuHB40 (Supplemental Fig. S9, A and B). The subcellular localization
294 analysis detected PuHB40 in the nucleus (Fig. 4L). Accordingly, PuHB40 is a
295 transcriptional factor localized in the nucleus.

296 **PuHB40 promotes *PuMYB123-like* transcript level**

297 On the basis of the presence of four possible PuHB40-binding sites in the *PuMYB123-like*
298 promoter (binding sites 1–4), we hypothesized that PuHB40 may modulate *PuMYB123-*
299 *like* expression by binding to its promoter. To test this hypothesis, we replaced the possible
300 binding sites with TTTTTTTTT. The dual-luciferase assay detected a significant decrease
301 in the activation of the *PuMYB123-like* promoter by PuHB40 when binding site 4 was
302 mutated (Fig. 5A). The electrophoretic mobility shift assay (EMSA) showed that PuHB40
303 can directly bind to the *PuMYB123-like* promoter fragment containing binding site 4 (Fig.
304 5B). The chromatin immunoprecipitation (ChIP) assay revealed the specific enrichment of

305 PuHB40 in the *PuMYB123-like* promoter region harboring binding site 4 (Fig. 5C). Thus,
306 PuHB40 likely activates *PuMYB123-like* expression by binding to site 4 in the *PuMYB123-*
307 *like* promoter.

308 To further verify the relationship between PuHB40 and *PuMYB123-like* expression,
309 we transiently overexpressed *PuHB40* and silenced *PuMYB123-like* in pear seedlings.
310 After a 3-day light treatment, anthocyanin accumulation was significantly greater in the
311 *PuHB40*-OE seedlings than in the control seedlings, but the positive effect of PuHB40 on
312 anthocyanin accumulation was significantly inhibited if *PuMYB123-like* was silenced (Fig.
313 5, D and E); a similar trend was detected in the expression of anthocyanin biosynthetic
314 genes (Fig. 5F). These results confirmed that PuHB40 promotes anthocyanin biosynthesis
315 in pear by regulating *PuMYB123-like* expression.

316 **PuHB40 positively regulates anthocyanin biosynthesis**

317 To analyze the PuHB40 function related to anthocyanin biosynthesis in pear, *PuHB40-*
318 overexpressing (*PuHB40*-OE) transgenic pear calli and *PuHB40*-RNAi pear calli were
319 generated. After a 2-day exposure to white light, the anthocyanin contents was higher in
320 the *PuHB40*-OE transgenic pear calli than in the control calli. Furthermore, anthocyanin
321 accumulation was barely detectable in the *PuHB40*-RNAi pear calli (Fig. 6A-C). A qPCR
322 analysis indicated that the anthocyanin-related genes *PcPAL*, *PcCHI*, *PcDFR*, *PcF3H*,
323 *PcANS*, *PcUFGT*, *PcMYB10* and *PcMYB123-like* were highly expressed in the *PuHB40-*
324 OE pear calli, whereas they were expressed at low levels in the *PuHB40*-RNAi pear calli

325 (Fig. 6D). In addition, *PuHB40* was ectopically expressed in *A. thaliana*. Compared with
326 the wild-type control, three independent transgenic lines ectopically overexpressing
327 *PuHB40* had higher anthocyanin contents (Fig. 6E-G) and shorter hypocotyls (Fig. 6H).
328 Moreover, the ectopic expression of *PuHB40* significantly increased the expression of
329 anthocyanin-related structural genes (Fig. 6I).

330 To further analyze the *PuHB40* function in pear fruits, bagged mature 'Zaosu' and
331 'Hongzaosu' pear fruits were used for transient overexpression and VIGS experiments,
332 respectively. The transient overexpression of *PuHB40* significantly promoted anthocyanin
333 biosynthesis in the pear peel (Supplemental Fig. S10, A and B), while also significantly
334 increasing the expression of anthocyanin biosynthetic genes and *PpMYB123-like*
335 (Supplemental Fig. S10C). However, compared with the control fruit peel, the *PuHB40*-
336 TRV fruit peel had a lower anthocyanin contents (Supplemental Fig. S10, D and E) and
337 lower anthocyanin biosynthetic genes and *PpMYB123-like* expression levels
338 (Supplemental Fig. S10F). Accordingly, PuHB40 may be involved in promoting
339 anthocyanin biosynthesis. Considered together, these results imply PuHB40 functions as a
340 positive transcriptional regulator governing anthocyanin production in pear.

341 **Identification of PuPP2AA2 and its interaction with PuHB40**

342 To further explore the mechanisms through which PuHB40 regulates ROS-dependent
343 anthocyanin biosynthesis under high-light stress, PuHB40-interacting proteins in pear
344 seedlings were identified via a GST pull-down assay followed by a mass spectrometry

345 analysis. Among the 36 identified proteins, we focused on the A subunit of PP2A
346 (Supplemental Table S4). According to a phylogenetic analysis, the PP2A A subunit
347 analyzed in the current study is most closely related to the A2 subunit of PP2A in *A.*
348 *thaliana.* Thus, it was named PuPP2AA2 (Fig. 7A). During the subcellular localization
349 analysis, PuPP2AA2 was detected in the nucleus and cytoplasm (Fig. 7B). The *PuPP2AA2*
350 expression level was significantly lower after the high-light treatment than after the DMTU
351 treatment (Fig. 7C). To investigate the response of PuPP2AA2 to ROS at the translational
352 level, we transiently overexpressed the fusion construct encoding MYC-tagged PuPP2AA2
353 (PuPP2AA2-MYC) in pear seedlings and then exposed the plants to high-light stress
354 conditions with or without a DMTU treatment. The PuPP2AA2 protein abundance
355 decreased sharply under high-light conditions, but the decrease was significantly
356 attenuated after the DMTU treatment, which presumably decreased the ROS level (Fig.
357 7D). Thus, PuPP2AA2 is inhibited by high-light stress-induced ROS.

358 The GST pull-down assay showed that PuHB40 can interact with PuPP2AA2 *in vitro*
359 (Fig. 7E), whereas the LCI and bimolecular fluorescence complementation (BiFC) assays
360 reflected the interaction between PuHB40 and PuPP2AA2 *in vivo* (Fig. 7, F and G). Taken
361 together, these data confirmed that PuHB40 interacts with the A2 subunit of PP2A,
362 PuPP2AA2, *in vitro* and *in viv*o.

363 **PuPP2AA2 inhibits PuHB40-dependent PuMYB123-like trans-activation by**
364 **dephosphorylating PuHB40**

365 To clarify whether the interaction between PuPP2AA2 and PuHB40 affects the
366 phosphorylation status of PuHB40, we transiently overexpressed the fusion construct
367 encoding GFP-tagged PuHB40 (PuHB40-GFP) in *Nicotiana benthamiana* leaves, which
368 were treated with cantharidin (i.e., a widely used PP2A inhibitor) (Honkanen 1993; Ren et
369 al. 2022). We also extracted proteins from the *N. benthamiana* leaves and separated them
370 in a Phos-tag gel and detected the fusion protein using an anti-GFP antibody. One of the
371 two bands detected in the gel corresponded to the phosphorylated form (P+) of PuHB40-
372 GFP, which migrated more slowly than the non-phosphorylated form (P−) of PuHB40-GFP.
373 Moreover, the P+:P− ratio increased after the cantharidin treatment (Fig. 8A), indicating
374 that the phosphorylation level increased after PP2A activity was inhibited. To further
375 investigate whether PP2A can directly dephosphorylate PuHB40, we purified the MYC,
376 PuHB40-GFP, and PP2A complex from pear seedlings that were transiently overexpressing
377 the constructs encoding MYC, PuPP2AA2-MYC, and PuHB40-GFP using MYC-Trap and
378 GFP-Trap agarose beads. Because PuPP2AA2 is a structural subunit that is tightly
379 associated with the B and C subunits of the PP2A holoenzyme, other PP2A subunits may
380 be co-purified in the PuPP2AA2-MYC immunoprecipitation complex (Zhou et al. 2004;
381 Ren et al. 2022). Thus, the PP2A complex co-purified by PuPP2AA2-MYC may contain
382 all of the subunits and have phosphatase activity (Ren et al. 2022). We incubated PuHB40-
383 GFP with the MYC and PP2A complex, after which different PuHB40-GFP isoforms were
384 detected using the anti-PuHB40 antibody for the Phos-tag analysis. The incubation with

385 the PP2A complex led to the dephosphorylation of PuHB40 and a decrease in the P+:P−
386 ratio from 0.57 to 0.27 (Fig. 8B), implying PP2A can directly dephosphorylate PuHB40.
387 To confirm that the phosphatase activity of PP2A was responsible for the decrease in the
388 phosphorylation of PuHB40, we deleted the last two tandem repeats (i.e., 14 and 15) of the
389 HEAT motif in the C-terminal of PuPP2AA2. The mutated sequence, which was named
390 PuPP2AA2D, was unable to bind to the B and C subunits of PP2A, thereby preventing the
391 formation of a functional holoenzyme (Ruediger et al. 1994). The subcellular localization
392 analysis showed that PuPP2AA2D was distributed in the nucleus as well as the cytoplasm,
393 similar to the distribution of PuPP2AA2 (Fig. 8C). The LCI and BiFC assays demonstrated
394 that the deletion of tandem repeats 14 and 15 did not affect the interaction between
395 PuPP2AA2D and PuHB40 (Fig. 8, D and E).

396 We transiently coexpressed the fusion constructs encoding PuHB40-GFP and
397 PuPP2AA2-MYC as well as the fusion constructs encoding PuHB40-GFP and MYC-
398 tagged PuPP2AA2D (PuPP2AA2D-MYC) in *N. benthamiana* leaves. Different isoforms
399 of PuHB40-GFP were detected by the Phos-tag analysis involving the anti-GFP antibody.
400 Furthermore, the extent of the phosphorylation of PuHB40 decreased significantly after the
401 overexpression of *PuPP2AA2* (i.e., significant decrease in the P+:P− ratio from 6.20 to
402 1.68), but there was no significant change in the phosphorylation of PuHB40 after the
403 overexpression of *PuPP2AA2D* (i.e., non-significant decrease in the P+:P− ratio from 6.20
404 to 5.83) (Fig. 8F). These results indicate PP2A can dephosphorylate PuHB40 *in planta*.

405 Hence, PP2A can dephosphorylate PuHB40 *in vivo* and *in vitro*. Finally, to determine
406 whether PuHB40 activity is influenced by its phosphorylation status, the PuHB40-induced
407 transcription of *PuMYB123-like* was determined in a dual-luciferase assay. The presence
408 of PuPP2AA2 abolished the ability of PuHB40 to activate *PuMYB123-like* transcription.
409 However, the lack of PP2A phosphatase activity had no significant effect on PuHB40-
410 activated *PuMYB123-like* transcription (Fig. 8G). Therefore, PuHB40 may interact with
411 PuPP2AA2, with the resulting dephosphorylation by PP2A affecting whether PuHB40 can
412 activate the transcription of *PuMYB123-like*.

413 **PP2A attenuates PuHB40-induced anthocyanin biosynthesis**

414 To elucidate the contribution of PuPP2AA2 to anthocyanin biosynthesis in pear, we
415 generated two *PuPP2AA2*-overexpressing transgenic pear calli lines (*PuPP2AA*2-OE #5
416 and #6), which were subsequently exposed to white light for three days. The anthocyanin
417 contents were much lower in *PuPP2AA2*-OE #5 and #6 than in the wild-type pear calli
418 (Fig. 9, A and B). The qPCR analysis indicated that the overexpression of *PuPP2AA2*
419 downregulated the expression of anthocyanin-related genes (Fig. 9C). We also transiently
420 silenced and overexpressed *PuPP2AA2* in pear fruit peels. At the injection site of the
421 *PuPP2AA2*-OE fruit peels, there was almost a complete lack of red coloration and the
422 anthocyanin contents was lower than that in the control fruit peels (Supplemental Fig. S11,
423 A and B). Moreover, the expression levels of anthocyanin-related genes were significantly
424 lower in the *PuPP2AA2*-OE pear fruit peels than in the control fruit peels (Supplemental

425 Fig. S11C). In contrast, the transient silencing of *PuPP2AA2* significantly promoted
426 anthocyanin accumulation (Supplemental Fig. S11, D and E) and increased the expression
427 of anthocyanin biosynthetic genes (Supplemental Fig. S11F) suggestive of the negative
428 regulatory effects of PuPP2AA2 on anthocyanin biosynthesis and the red coloration of pear
429 fruits.

430 To assess whether the phosphorylation status of PuHB40 affects its function
431 associated with ROS-induced anthocyanin biosynthesis in pear, we transiently
432 overexpressed *PuHB40* alone as well as with *PuPP2AA2* in pear seedlings, which were
433 then subjected to a 2-day light treatment. Anthocyanin accumulation and the expression of
434 anthocyanin-related genes as well as *PuMYB123-like* were greater in the pear seedlings
435 overexpressing *PuHB40* alone than in the control seedlings. In contrast, there were no
436 obvious differences in anthocyanin accumulation and the expression of the related genes
437 between the control pear seedlings and the seedlings coexpressing *PuHB40* and *PuPP2AA2*
438 (Fig. 9, D-F). Additionally, bagged mature 'Hongzaosu' pear fruits were used for the
439 transient overexpression of *PuHB40* alone and with *PuPP2AA2*. Compared with the
440 corresponding control levels, the anthocyanin contents and the expression levels of
441 anthocyanin-related genes increased significantly in the pear fruit peels overexpressing
442 *PuHB40* alone, but the presence of PuPP2AA2 weakened the effects of PuHB40 on
443 anthocyanin biosynthesis and the expression of the related genes (Fig. 9, G-I). Thus, the
444 dephosphorylation of PuHB40 by PP2A adversely affects anthocyanin biosynthesis.

445 **DISCUSSION**

446 Plants growing under natural conditions over long periods are increasingly becoming more
447 susceptible to different stresses because of the variability in environmental conditions due
448 to global warming and climate change (Lesk et al. 2016). In plant cells, stress can induce
449 the rapid accumulation of ROS, which are important signaling molecules that activate plant
450 mechanisms related to defense and acclimatization (Mittler et al. 2022). High-light stress-
451 induced ROS accumulation is closely related to photosynthetic activities. Under high-light
452 conditions, chlorophylls are converted to their excited state following the absorption of
453 light energy. The subsequent increase in electron transfer and energy dissipation eventually
454 leads to the formation of highly activated triplet excited chlorophylls that readily transfer
455 excitation energy to O_2, which forms O_2^- and H_2O_2 in photosystem I and $^1O_2$ in
456 photosystem II (Asada 2006; Foyer and Noctor 2009; Li et al. 2009; Mullineaux et al.
457 2018). Additionally, high-light stress can also induce ROS accumulation in a
458 photosynthesis-independent manner in plant cells lacking photosynthetic pigments via a
459 process mediated by NADPH oxidase (Xiong et al. 2021). Excessive amounts of ROS can
460 damage plant cells and may lead to cell death (Mittler 2017) In response to a wide range
461 of stresses and to maintain ROS homeostasis, plants have evolved a series of mechanisms,
462 including those mediating anthocyanin accumulation.

463 In plants, anthocyanins are crucial antioxidants that function as ROS scavengers
464 (Gould et al. 2002; Neill et al. 2002; Bi et al. 2014; Jiang et al. 2023). Many studies showed

465 that anthocyanin accumulation is strongly induced by various stresses, such as high-light
466 stress, ultraviolet radiation, and low temperatures (Steyn et al. 2002; Catalá et al. 2011; Xie
467 et al. 2012; Nakabayashi et al. 2014; Landi et al. 2015; Xu et al. 2015). An earlier
468 investigation involving raman spectroscopy confirmed that abiotic stress conditions
469 increase the ROS and anthocyanin contents in the leaves of coleus plants (Altangerel et al.
470 2017). However, the link between ROS and anthocyanins remains unclear. Although
471 treating *A. thaliana* seedlings with H_2O_2 and ROS activators promotes anthocyanin
472 accumulation (Xu et al. 2017; Shi et al. 2018), evidence of the relationship between ROS
473 and anthocyanin accumulation is lacking. In this study, the ROS scavenger DMTU was
474 applied to eliminate ROS induced by various stresses, thereby serving as a reliable negative
475 control. Stress-induced anthocyanin accumulation in pear seedlings was attenuated by
476 DMTU (Fig. 1, A and B; Supplemental Fig. S1A), indicating that the increase in the
477 anthocyanin contents depends on ROS, which likely function as signaling molecules
478 linking the exposure to different stresses to changes in anthocyanin contents.

479 Anthocyanin biosynthesis is regulated by the MBW complex, with MYB TFs playing
480 a major role and responding to various environmental and internal factors (Xu et al. 2015).
481 R2R3-MYB proteins of subgroup 6 is responsible for anthocyanin biosynthesis (Dubos et
482 al. 2010). In rosaceous plants, MYB10 TFs, which belong to subgroup 6, are essential
483 promotors of light-induced anthocyanin biosynthesis (Takos et al. 2006; Espley et al. 2007;
484 Feng et al. 2010). Although most of the MYB TFs promoting anthocyanin biosynthesis

485 belong to subgroup 6, a few members of other subgroups are also involved. For example,
486 the subgroup 2 members MdMYB9 and MdMYB11 promote jasmonic acid-induced
487 anthocyanin biosynthesis by increasing the expression of anthocyanin-related structural
488 genes (An et al. 2015), whereas MdMYB308L, which is a member of subgroup 4, promotes
489 low-temperature-induced anthocyanin biosynthesis by interacting with MdbHLH33 (An et
490 al. 2020). In the current study, we determined that PuMYB123-like, which belongs to
491 subgroup 5, is the key MYB TF mediating anthocyanin biosynthesis via the ROS-
492 responsive pathway. Traditionally, PuMYB10 has been considered the main MYB TF
493 responsible for anthocyanin biosynthesis in pear (Feng et al. 2010; Bai et al. 2019a),
494 however, its expression is similar following the high-light stress and DMTU treatments
495 (Fig. 1M). The MYB subgroup 5 members are primarily involved in proanthocyanidin
496 biosynthesis, but in the present study, the overexpression of *PuMYB123-like* did not affect
497 proanthocyanidin accumulation in pear calli (Supplemental Fig. S6A). Instead,
498 PuMYB123-like promoted anthocyanin biosynthesis by interacting with PubHLH3 (Fig.
499 2). Our study findings suggest that members of other MYB subgroups may also have
500 important regulatory effects on anthocyanin biosynthesis, further clarifying the
501 involvement of MYB TFs in ROS-associated anthocyanin biosynthesis.

502 According to earlier research, HD-Zip I family members are crucial regulators of plant
503 responses to stress, especially drought and osmotic stress (Ariel et al. 2007; Harris et al.
504 2011). But their role in other stresses is less well known. However, their roles in responses

505 to other stresses are less well known. In this study, one HD-Zip I family member, which
506 was designated as PuHB40 on the basis of previously reported nomenclature (Yang et al.
507 2018), was identified as a key TF involved in ROS-regulated anthocyanin biosynthesis
508 under high-light stress conditions (Fig. 4). Considering the importance of HD-Zip I family
509 members in various stress responses, PuHB40-regulated high-light stress-induced
510 anthocyanin biosynthesis might be a universal response to diverse stresses. The response
511 of HD-Zip I TFs to drought stress depends on abscisic acid (ABA) (Söderman et al. 1996;
512 Söderman et al. 1999; Olsson et al. 2004), but the relationship with ROS remains unknown.
513 In the current study, PuHB40 responded to high-light stress in an ROS-dependent manner
514 (Fig. 4F), implying HD-Zip I TFs can respond to other abiotic stresses (i.e., in addition to
515 drought) through multiple signaling pathways. The stability and activity of HD-Zip
516 proteins are regulated by phosphorylation. In apple, MdHB1 and MdHB2 are
517 phosphorylated by SnRK2, thereby enhancing their stability and activity, which leads to
518 increased *MdACO1* expression and ethylene biosynthesis (Jia et al. 2022). In *A. thaliana*,
519 ATHB6 is dephosphorylated by the PP2C phosphatase ABI1, which functions as a negative
520 regulator in the ABA signaling pathway (Himmelbach et al. 2002). The phosphorylation
521 status of HD-Zip I TFs is mainly influenced by the ABA signaling pathway. In the present
522 study, the phosphorylation of PuHB40 was regulated by ROS via PP2A (Fig. 8). The
523 decrease in the extent of the phosphorylation of PuHB40 decreased the PuHB40-activated
524 transcription of *PuMYB123-like*, ultimately decreasing ROS-induced anthocyanin

525 biosynthesis (Fig. 9, D and G). In plants, PP2A is a ubiquitous and highly conserved
526 serine/threonine-specific phosphatase (Farkas et al. 2007) that catalyzes
527 dephosphorylations with diverse regulatory effects on plant stress responses (Lillo et al.
528 2014). In general, under salt and osmotic stress conditions, PP2A is inhibited, resulting in
529 phosphorylated target proteins that help protect against various stresses (Bian et al. 2020;
530 Li et al. 2020). However, the effects of ROS on PP2A phosphatase activity under abiotic
531 stress conditions are unclear. In this study, we observed that the structural subunit of PP2A
532 was repressed by ROS in pear (Fig. 7, C and D), suggesting that the regulatory effects of
533 PP2A on plant stress responses may involve ROS. The A subunit of PP2A is the structural
534 subunit that provides a scaffold that binds to the B and C subunits (Kamibayashi et al. 1992;
535 Ruediger et al. 1994; Groves et al. 1999; Janssens and Goris 2001). In *A. thaliana*, three A
536 subunits of PP2A have been identified (RCN1, PP2AA2, and PP2AA3). A mutation to
537 RCN1 results in severe phenotypic changes, including stunted growth (dwarfism),
538 abnormal embryogenesis, and sterility. This is in contrast to the mostly normal phenotypes
539 of the *pp2aa2* and *pp2aa3* mutants (Zhou et al. 2004). Thus, it is widely believed that
540 RCN1 is critical for the overall regulation of PP2A, which may help to explain why there
541 have been relatively few studies on PP2AA2 and PP2AA3 (Lillo et al. 2014). In the current
542 study, we revealed that PuPP2AA2 affects ROS-induced anthocyanin biosynthesis by
543 dephosphorylating PuHB40 (Fig. 10), which clarifies the role of the A subunit of PP2A in
544 plants and highlights the importance of the other A subunits.

545 In summary, PuHB40 is the key TF regulating ROS-induced anthocyanin biosynthesis.
546 Specifically, it is a transcriptional activator that induces PuMYB123-like/PubHLH3
547 complex for anthocyanin biosynthesis. The ability of PuHB40 to activate target gene
548 transcription depends on its phosphorylation level, which is regulated by PP2A.
549 Furthermore, ROS accumulation leads to the extensive phosphorylation of PuHB40 by
550 suppressing the transcription of *PuPP2AA2*, thereby enhancing the PuHB40-activated
551 transcription of *PuMYB123-like* and promoting anthocyanin biosynthesis (Fig. 10). Our
552 study findings have elucidated the molecular mechanisms by which abiotic stresses
553 regulate anthocyanin biosynthesis in pear, providing insights into how ROS modulate
554 anthocyanin biosynthesis.
555

556 **MATERIALS AND METHODS**

557 **Plant materials and treatment**

558 The sterile seedlings of 'Qingzhen No. 1' pear (*Pyrus ussuriensis*) were kindly provided
559 by Professor Ran Wang of Qingdao Agricultural University. The pear seedlings were
560 growth at 25°C under a 16 h light/ 8 h dark photoperiod (photon flux density 50 μmol·s^{-}
561 ^{1}·m^{-2}). For high-light treatment, pear seedlings were exposed to continuous LED white
562 light (photon flux density 160 μmol·s^{-1}·m^{-2}) in a growth chamber. For salt and drought
563 stress, pear seedlings were growth on solid MS medium supplemented with 30 mM sodium
564 chloride or 2.5% polyethylene Glycol 8000 (PEG 8000) respectively and were exposed to

565 continuous LED white light (photon flux density 50 μmol·s^{-1}·m^{-2}). For N, N'-
566 dimethylthiourea (DMTU) treatment, seedlings were growth on solid MS medium
567 supplemented with 5 mM DMTU and other conditions are same as corresponding stress
568 treatment. After treatment, the seedlings were collected, immediately frozen in liquid
569 nitrogen, and stored at -80°C until used.

570 Pear calli were generated from the flesh of 'Clapp's Favorite' (*Pyrus communis*)
571 fruitlets as previously described (Bai et al. 2019b). For H_2O_2 treatment, pear calli in good
572 condition were firstly grown on the MS solid medium supplemented with 4 mM H_2O_2 for
573 overnight and then were exposed to continuous white light (photon flux density 160
574 μmol·s^{-1}·m^{-2}) for two days at 17°C. The pear calli were collected after treatment and stored
575 at -80°C until used.

576

577 **Measurement of the total anthocyanin contents**

578 The measurement of anthocyanin contents is as previously described (Zhang et al. 2022).
579 Briefly, 0.1 g powder of pear seedlings, pear calli or pear peels were soaked in 500 μL
580 methanol: hydrochloric acid (99:1, v/v) solution and incubated overnight at 4°C in darkness.
581 For pear seedlings, 250 μL chloroform and 250 μL double distilled water were added to the
582 extracting solution for mixing and centrifuged for 10 minutes (4°C, 12000 rpm). The
583 supernatant was measured at 530, 657 nm using the DU800 spectrophotometer (Beckman
584 Coulter, Brea, CA, USA). The anthocyanin contents was calculated using the formula:

585 $(A_{530}-0.25*A_{657})/0.1$.

586 For pear calli and peels, the extracting solution was centrifuged at 4°C, 12000 rpm,
587 for 10 minutes. And then, the absorbance of supernatant was measured at 530, 620, and
588 650 nm using the DU800 spectrophotometer (Beckman Coulter, Brea, CA, USA). The
589 anthocyanin contents was calculated using the formula $([A_{530}-A_{650}]-0.2\times[A_{650}-A_{620}])/0.1$.

590

591 **Histological staining detection of ROS**

592 H_2O_2 and O_2^- were detected as previously described with minor modification (Xu et al.
593 2017). Briefly, the leaves of pear seedlings were dipped in DAB staining solution (for H_2O_2
594 detection) containing 1 $mg\cdot ml^{-1}$ DAB or NBT staining solution (for O_2^- detection)
595 containing 1 $mg\cdot ml^{-1}$ NBT. The leaves were incubated overnight in the dark with gentle
596 shaking (25°C, 220 $rpm\cdot min^{-1}$). Then, the chlorophyll of leaves was removed by incubating
597 with bleaching solution (ethanol: acetic acid: glycerol=3:1:1) at 85°C for 30 min. Finally,
598 the leaves were kept in preservative solution (ethanol: glycerol = 4: 1) until images taken.

599

600 **RNA isolation and reverse transcription quantitative PCR**

601 Total RNA was extracted with a modified CTAB method (Zhang et al. 2012). After
602 genomic DNA removed, the first-strand cDNA was synthesized from 1 μg RNA with
603 HiScript II First Strand cDNA Synthesis Kit (+gDNA wiper; Vazyme Biotech, China).
604 qPCR was conducted using ChamQ SYBR qPCR Master Mix (Vazyme, China) on CFX
605 Connect real-time PCR system (Bio-Rad, https://www. bio-rad.com/). The relative

606 expression levels of genes were calculated using the $2^{-\triangle\triangle Ct}$ method (Livak and Schmittgen
607 2001) with the pear *PpActin* gene (GenBank accession no. JN684184) to normalize the
608 expression values, and the analyses were carried out with three biological replicates. The
609 primers for RT-qPCR are listed in Supplemental Data Set S2.
610
611 **H_2O_2 content quantification**
612 The powder of pear seedlings leaves was soaked in 1 ml of 20 mM potassium phosphate
613 buffer (pH 6.5) on ice and centrifuged (4°C, 1000 rpm), then the supernatant was
614 transferred to new centrifuge tubes (2 ml) and additional potassium phosphate buffer was
615 added to 1.5 ml. 100 μL plant extract was used in each reaction and the H_2O_2 concentration
616 was measured with the Amplex Red hydrogen peroxide/peroxidase assay kit (Thermo
617 Fisher Scientific, Cat. No. A22188).
618
619 **Subcellular localization analysis**
620 Subcellular localization analysis was performed as previously described (Ni et al. 2023).
621 the full-length complete coding sequences (CDS) (without termination codons) of the
622 target genes (*PuMYB123-like*, *PuHB40*, *PuPP2AA2* and *PuPP2AA2D*) were inserted into
623 pCAMBIA1300 vector to produce *Pro35S: PuMYB123-like-GFP*, *Pro35S: PuHB40-GFP*,
624 *Pro35S: PuPP2AA2-GFP*, and *Pro35S: PuPP2AA2D-GFP*, respectively. *Agrobacterium*
625 strain GV3101 harboring the plasmids were infiltrated into the leaves of *N. benthamiana*
626 transgenic lines containing red fluorescent protein in the nuclei. The GFP and mCherry

627 fluorescence signals were observed by confocal laser scanning microscopy (A1, Nikon,
628 Tokyo, Japan). The primers used for vector construction are listed in Supplemental Data
629 Set S1.
630
631 **Transient transformation assay in pear fruits and seedlings**
632 'Hongzaosu' (also called 'Red Zaosu') pear fruits (*Pyrus pyrifolia* × *Pyrus communis*,
633 genes from it are prefixed with 'Pp') were collected from the orchard at the Institute of
634 Horticulture, Henan Academy of Agricultural Sciences, Henan, China. Fruits were covered
635 with lightproof double-layered paper bags during the growing season and were harvested
636 about 140 d after full bloom, then immediately transported to the laboratory with the bags.
637 Transient transformation assay in pear fruits was performed as previously described (Ni et
638 al. 2023). For the transient overexpression, the full-length CDS of *PuMYB123-like*,
639 *PuHB40* and *PuPP2AA2* was cloned to the pGreenII 0029 62-SK vector and their
640 expression was driven by the 35S promoter. Pear fruits were infiltrated with *A. tumefaciens*
641 GV3101 cells containing the plasmid by a needle syringe. For VIGS assay, the gene
642 fragment (~200 to 300 bp) was inserted into the pTRV2 vector (gene-pTRV2) and
643 transformed into *A. tumefaciens* GV3101. Gene-pTRV2 or empty pTRV2 (negative control)
644 was mixed with pTRV1 in equal proportions and co-infiltrated into pear fruits by a needle
645 syringe. After infiltration, pear fruits were exposed to continuous white light (160 $\mu mol \cdot m^{-2} \cdot s^{-1}$)
646 and UV-B light (1.1 $\mu mol \cdot m^{-2} \cdot s^{-1}$). The fruit peel surrounding the injection sites was

647 collected and stored at -80°C until use.

648 For transient transformation assay in pear seedlings, the full-length CDS of *PuHB40*,
649 *PuPP2AA2* (for overexpression) and reverse complementary gene fragment (~200 to 300
650 bp) of *PuMYB123-like* (*PuMYB123-like-RNAi*, for gene silencing) were cloned to
651 pCAMBIA1301, and then the plasmids were transformed into *A. tumefaciens* GV3101. *A.*
652 *tumefaciens* GV3101 containing *PuHB40* was mixed with empty pCAMBIA1301,
653 *PuMYB123-like-RNAi*, or *PuPP2AA2* in equal proportions and co-infiltrated into seedlings
654 by vacuum (0.8 $kg \cdot cm^{-2}$, 5 min). The seedlings were then recovered in darkness (25°C) for
655 1~2 d and then transferred to a growth chamber for treatment under continuous white light
656 (photon flux density 160 $\mu mol \cdot s^{-1} \cdot m^{-2}$). Finally, the seedlings were collected, frozen in
657 liquid nitrogen immediately, and stored at -80°C until used. The primers used for vector
658 construction are listed in Supplemental Data Set S1.

659

660 **Genetic transformation of pear calli**

661 Transgenic pear calli were generated as previously described (Bai et al. 2019b). Briefly,
662 pear calli were soaked with *A. tumefaciens* EHA105 containing different vectors (PuHB40-
663 pCAMBIA1301, PuMYB123-like-pCAMBIA1301, PuPP2AA2-pCAMBIA1301 for
664 overexpression and PuHB40-RNAi-pCAMBIA1301, PuMYB123-like-RNAi-
665 pCAMBIA1301 for silencing) for 12~15 min and then co-cultured on MS solid medium
666 for 2 d in darkness. Positive pear calli were screened on solid MS medium supplemented
667 with antibiotics (10 mg/L hygromycin B) under continuous darkness at 25°C for 1~3

668 months and subcultured every 3 weeks. For light treatment, pear calli in good condition
669 were exposed to continuous white light (photon flux density 160 $\mu mol \cdot s^{-1} \cdot m^{-2}$). The
670 primers used for vector construction are listed in Supplemental Data Set S1.
671
672 **Yeast two-hybrid assays (Y2H)**
673 The Y2H assay was carried out based with the manufacturer's protocol of Matchmaker
674 Gold Yeast Two-Hybrid System Kit (Takara). The primers used for vector construction are
675 listed in Supplemental Data Set S1.
676
677 **Pull down screening coupled with LC-MS/MS**
678 The full-length CDS of *PuHB40* was cloned to the pGEX-4T-1 vector. Then, the GST-
679 tagged PuHB40 protein (PuHB40-GST) bound to GST-Trap agarose beads (Yeasen,
680 Shanghai, China) were incubated with total proteins of pear seedlings at 4°C for overnight,
681 the GST bound to GST-Trap agarose beads were used as negative control. The PuHB40-
682 GST and GST proteins were eluted by glutathione with gravity column and subjected to
683 immunoblotting analysis with anti-GST antibody (Cowin Biotech, China, CW0084M). The
684 eluent solution was further analyzed by mass spectrometry.
685 For pull-down assay, His-tagged PuMYB123-like were incubated with GST or GST-
686 tagged PubHLH3 in equal proportions for overnight at 4°C. Similarly, His-tagged PuHB40
687 were incubated with GST or GST-tagged PuPP2AA2 in equal proportions for overnight at
688 4°C. Then the proteins were eluted by glutathione and the eluents were subjected to

689 immunoblotting analysis with anti-GST antibody and anti-His antibody (Cowin Biotech,
690 China, CW0286M). The primers used for vector construction are listed in Supplemental
691 Data Set S1.
692
693 **Luciferase complementation imaging assays**
694 The coding sequences (without termination codons) of *PuHB40*, *PubHLH3* was inserted
695 into pCAMBIA1300-nLUC vectors, and the CDS of *PuMYB123-like*, *PuPP2AA2* and
696 *PuPP2AA2D* was cloned to pCAMBIA1300-cLUC vectors. The vectors were introduced
697 into *Agrobacterium* strain GV3101 individually and *A. tumefaciens* harboring gene-nLUC
698 were mixed with an equal volume of *Agrobacteria* containing gene-cLUC and then co-
699 infiltrated into *N. benthamiana* leaves. Five minutes before detection, 10 mM firefly
700 luciferin (Promega) was injected into the same position as the agrobacteria infiltration and
701 the iluminescence was captured by ChemiDoc™XRS+ (Bio-Rad). *N. benthamiana* leaves
702 were co-infiltrated with gene-cLUC and nLUC or cLUC and gene-nLUC as the negative
703 control. The primers used for vector construction are listed in Supplemental Data Set S1.
704
705 **Bimolecular fluorescence complementation assay (BIFC)**
706 BIFC assay was performed as previously described (Hu et al. 2002; Walter et al. 2004).
707 The full-length *PuHB40* was inserted into p2YC and p2YN, while *PuPP2AA2* and
708 *PuPP2AA2D* were cloned to p2YN and p2YN respectively. Then, *A. tumefaciens* GV3101
709 cells harboring gene-p2YN and gene-p2YC were mixed in equal proportions and co-

710 infiltrated into *N. benthamiana* leaves by injection, leaves were co-infiltrated with gene-
711 2YN and 2YC or 2YN and 2YC-gene as the negative control. The YFP signal was detected
712 by a confocal laser scanning microscope (A1, Nikon, Tokyo, Japan) after 48 h~72 h. The
713 primers used for vector construction are listed in Supplemental Data Set S1.
714
715 **Dual-luciferase assay**
716 Dual-luciferase assays were performed as previously reported (Bai et al. 2019a). The full-
717 length CDS of *PuHB40*, *PuPP2AA2* and *PuPP2AA2D* were cloned into pGreenII 0029 62-
718 SK vector (gene-SK) and the fragments of *PuMYB123-like* promoter were ligated into
719 pGreenII 0800-LUC vector (promoter-LUC). All vectors were transformed into *A.*
720 *tumefaciens* strain GV3101 cells harboring the pSoup vector. *A. tumefaciens* strain GV3101
721 containing gene-SK and promoter-LUC were injected into *N. benthamiana* leaves at a ratio
722 of 1:10. The firefly luciferase and Renilla luciferase activities were analyzed at 48 h after
723 the infiltration by the Dual-Luciferase Reporter Assay System (Promega) and the
724 GloMax96 Microplate Luminometer (Promega). The primers used for vector construction
725 are listed in Supplemental Data Set S1.
726
727 **Electrophoretic mobility shift assay**
728 The 3' end biotin-labeled double-stranded DNA probes were prepared by annealing 3' end
729 biotin-labeled oligonucleotides to the corresponding complementary strands (95 °C for 5

730 min and 70 °C for 20 min). The EMSA were performed using the Light-Shift™
731 Chemiluminescent EMSA Kit (Thermo Scientific) following the manufacturer's protocol.
732 Briefly, 3 μg recombinant PuHB40-His protein was incubated with labeled (2 nM) or
733 nonlabelled (6 nM, 10 nM, 20 nM) double-stranded probes at room temperature,
734 respectively, for 20 min in binding buffer. The samples were then separated by 6.5% (w/v)
735 native polyacrylamide gels at 4 °C and the biotin-labeled probes was captured with
736 ChemiDoc™XRS+ (Bio-Rad). The oligonucleotide probes used in this study are listed in
737 Supplemental Data Set S1.
738
739 **ChIP-qPCR assay**
740 The ChIP-qPCR assays were performed as previously described (Ni et al. 2023). The pear
741 calli transformed with the recombinant PuHB40-MYC construct and the empty construct
742 (MYC alone) were prepared for ChIP assays. The pear calli were treated in 1% (w/v)
743 formaldehyde under vacuum for 10 min for the cross-linking and then the chromatin was
744 extracted via sucrose gradient centrifugation. The chromatin DNA was sonication for 30
745 min on ice (30 s with 30 s intervals) with the Bioruptor Plus device (Diagenode) to shear
746 the chromatin to an average size of 200 bp to 500 bp. The sheared chromatin was incubated
747 with Anti-MYC (Sigma-Aldrich, 05-724) at 4°C overnight and the amount of
748 immunoprecipitated chromatin was determined by qPCR. Each ChIP assay was repeated 3
749 times, and the enriched DNA fragments in each ChIP sample served as 1 biological

750 replicate for qPCR. The primers used for the ChIP-qPCR analysis are listed in
751 Supplemental Data Set S3.
752
753 **Mn^{2+}-Phos-tag SDS-PAGE**
754 Prior to Phos-tag analysis, total protein extracted from pear leaves were pretreated by TCA
755 precipitation and then protein samples were separated by 10% regular SDS-PAGE gel
756 supplemented with 60 μM Phos-tag (TM) Acrylamide AAL-107 (Wako) and 120 μM
757 $MnCl_2$. The electrophoresis was carried out for 1.5 h using Mini Trans-Blot Electrophoretic
758 Transfer Cell (#1703930, BIO-RAD, USA). The gel was washed by gently agitating for 10
759 minutes for 3 times using general transfer buffer supplemented with 10 mmol/L EDTA and
760 then washed by general transfer buffer for 10 min. Finally, the gels were used for
761 immunoblotting analysis.
762
763 ***In vitro* and *in vivo* protein dephosphorylation assays**
764 For *in vitro* dephosphorylation assays, *A. tumefaciens* GV3101 harboring PuHB40-GFP,
765 PuPP2AA2-MYC and MYC were infiltrated into pear seedlings by vacuum (0.8 $kg \cdot cm^{-2}$,
766 5 min). Then, PuHB40-GFP, PuPP2AA2-MYC and MYC were purified by
767 immunoprecipitation from pear seedlings with GFP-Trap and MYC-Trap agarose beads.
768 Purified PuPP2AA2-MYC was considered as PP2A complex, since other subunits of PP2A
769 could co-immunoprecipitated with PuPP2AA2 (Zhou et al. 2004; Ren et al. 2022). Equal

770 volume of purified PuHB40-GFP mixed with PuPP2AA2-MYC or MYC were then
771 incubated in an oscillator (1200 g, 30 °C) for 2 h. The reaction was terminated by adding
772 protein loading buffer and boiled at 98 °C for 10 min. Finally, the mixtures were used for
773 immunoblotting analysis with anti-MYC monoclonal antibody (Cowin Biotech, China,
774 CW0299M), anti-GFP polyclonal antibody (HuaBio, China, R1312-2) and anti-PuHB40
775 (ABclonal Technology, Woburn, USA).

776 For *in vivo* dephosphorylation assays, *A. tumefaciens* GV3101 harboring PuHB40-
777 GFP was mixed with *A. tumefaciens* GV3101 harboring MYC, PuPP2AA2-MYC,
778 PuPP2AA2D-MYC in equal proportions and co-infiltrated into *N. benthamiana* leaves by
779 injection. The total proteins were extracted from *N. benthamiana* leaves after 48 h-72 h and
780 subjected to TCA precipitation, immediately followed by Phos-tag analysis. For
781 cantharidin treatment, *A. tumefaciens* GV3101 with PuHB40-GFP was infiltrated into *N.*
782 *benthamiana* leaves for 24 h. Then, 50 μM cantharidin was injected into the same position
783 as the agrobacteria infiltration and waited for 24 h. Finally, the total proteins were extracted
784 and then used for Phos-tag analysis.

785

786 **The preparation of PuHB40-specific antibody**

787 An affinity-purified anti-PuHB40 polyclonal antibody was generated by ABclonal
788 Technology (Woburn, USA) with the specific fragment of *in vitro* expressed PuHB40 (60-
789 215 aa) amplified from cDNA of pear seedling (*Pyrus ussuriensis*).

790

791 **Sequence analysis and phylogenetic analysis**

792 Protein sequence alignments were performed using MEGA X software (Kumar et al. 2018)
793 with default parameters. The phylogenetic tree was constructed via the maximum-
794 likelihood method in MEGA X software. The protein sequence alignments used to
795 construct the phylogenetic tree are provided in Supplemental File S1/S3/S5/S7, and the
796 tree files are provided in Supplemental File S2/S4/S6/S8.

797

798 **RNA-seq data analysis**

799 The library construction and sequencing were performed by Novogene (Beijing, China) on
800 an Illumina Novaseq platform with a 150-bp pair-end strategy. Clean data was obtained
801 from the raw data by eliminating low-quality reads as well as reads containing an adapter
802 or poly-N sequences and were mapped to reference genome of 'Cuiguan' pear (Gao et al.
803 2021). The expression levels of genes were calculated based on FPKM. The DETs were
804 identified by differential gene expression analysis tool of TBtools-II (Chen et al. 2023).
805 The obtained *P*-values were adjusted based on Benjamini and Hochberg method, and the
806 genes with adjusted *P*-values less than 0.05 were finally identified as differentially
807 expressed genes (fold-change $\geqslant$ 2, false discovery rate < 0.01).

808

809 **Statistical analysis**

810 All data in this study were analyzed using two-sided Student's *t*-test or one-way analysis

811 of variance (ANOVA) to determine statistical significance with GraphPad Prism v.9.0.
812 Detailed statistical analysis data are shown in Supplemental Data Set S7.
813

814 **ACCESSION NUMBERS**

815 The RNA sequencing data have been deposited in the NCBI Sequence Read Archive
816 (http://www.ncbi.nlm.nih.gov/sra/), with the BioProject ID: PRJNA1098349. Sequence
817 data of genes from this article can be found in an online pear genome database
818 (https://ngdc.cncb.ac.cn/gwh/Assembly/18534/show): PuHB40 (EVM0020592.1),
819 PuMYB123-like (EVM0034726.1), PuPP2AA2 (EVM0003533.1), PubHLH3
820 (EVM0031731.1), PubHLH33 (EVM0038434.1), PubHLH64 (EVM0003136.1), PuELIP1
821 (EVM0019834.1), PuELIP2 (EVM0035306.1), PuCHS (EVM0036585.1), PuCHI
822 (EVM0024725.1), PuF3H (EVM0021098.1), PuDFR (EVM0012887.1), PuANS
823 (EVM0001840.1), PuUFGT (EVM0026501.1), PuMYB10 (EVM0039871.1), PuMYB114
824 (EVM0020507.1).
825

826 **SUPPLEMENTAL DATA**

827 **Supplemental Figure S1**. Stresses induced anthocyanin biosynthesis is ROS-dependent
828 (Supports Figure 1).

829 **Supplemental Figure S2.** Identification of transcripts by the weighted gene co-expression
830 network analysis (WGCNA) of high-light stress-treated or high-light stress supplemented

831 with DMTU treatment in pear seedlings (Supports Figure 2).

832 **Supplemental Figure S3**. Expression levels of eight R2R3-MYB TFs in "purple" module

833 in pear seedlings treated with high-light stress or high-light stress supplemented with

834 DMTU (Supports Figure 2).

835 **Supplemental Figure S4.** Identification of PuMYB123-like (Supports Figure 2).

836 **Supplemental Figure S5.** The interaction between PuMYB123-like and PubHLHs

837 (Supports Figure 2).

838 **Supplemental Figure S6.** Functional analysis of PuMYB123-like in 'Hongzaosu' and

839 'Zaosu' pear fruit (Supports Figure 3).

840 **Supplemental Figure S7.** Results of the Mfuzz clustering of 11,608 differentially

841 expressed transcripts based on their expression patterns (Supports Figure 4).

842 **Supplemental Figure S8.** Detection of anti-PuHB40 polyclonal antibody specificity

843 (Supports Figure 4).

844 **Supplemental Figure S9.** Identification of PuHB40 (Supports Figure 4).

845 **Supplemental Figure S10**. Functional analysis of PuHB40 in 'Hongzaosu' and 'Zaosu'

846 pear fruit (Supports Figure 6).

847 **Supplemental Figure S11.** Functional analysis of PuPP2AA2 in 'Hongzaosu' pear fruit

848 (Supports Figure 9).

849 **Supplemental Data Set S1.** Primers used for constructing vectors or EMSA in this study.

850 **Supplemental Data Set S2.** Primers for qPCR analysis in this study.

851 **Supplemental Data Set S3.** Primers for ChIP-qPCR analysis in this study.

852 **Supplemental Data Set S4.** PuHB40 possible interacting proteins were identified with

853 GST pull-down combined with mass spectrometry.

854 **Supplemental Data Set S5.** The FPKM value and annotations of genes in "purple" module.

855 **Supplemental Data Set S6.** The FPKM value and annotations of DETs in cluster 14.

856 **Supplemental Data Set S7.** Detailed statistical analysis in this study.

857 **Supplemental File S1.** Protein sequences used to generate phylogenetic tree in Fig. 2B.

858 **Supplemental File S2.** Phylogenetic tree of Fig. 2B in Newick format.

859 **Supplemental File S3.** Protein sequences used to generate phylogenetic tree in Fig. 7A.

860 **Supplemental File S4.** Phylogenetic tree of Fig. 7A in Newick format.

861 **Supplemental File S5.** Protein sequences used to generate phylogenetic tree in Fig. S4A.

862 **Supplemental File S6.** Phylogenetic tree of Fig. S4A in Newick format.

863 **Supplemental File S7.** Protein sequences used to generate phylogenetic tree in Fig. S9A.

864 **Supplemental File S8.** Phylogenetic tree of Fig. S9A in Newick format.

865

866 **ACKNOWLEDGMENTS**

867 We thank R. Wang at Qingdao Agricultural University for providing pear seedlings of

868 'Qingzhen No. 1' (*Pyrus ussuriensis*). We also thank Kunfeng Li for technical help and

869 providing plant materials.

870

871 **FUNDING INFORMATION**

872 This work was supported by the Zhejiang Provincial Natural Science Foundation of China
873 under Grant No. LR22C150001, The National Natural Science Foundation of China
874 (32072545 to YT, 32272639 to SB, 32260745 to JS), and the China Agriculture Research
875 System of MOF and MARA.

876

877 **AUTHOR CONTRIBUTIONS**

878 Y.T and S.B. planned the work. S.B. and L.Z. conceived and designed the experiments.
879 L.Z. performed most experiments. L.W., S.Y. helped conduct some of the experiments. Y.F.,
880 Y.G. and J.S. helped to analyze the data. L.Z. and S.B wrote the manuscript and, Y.T., J.N.
881 helped to revise the manuscript. All authors read and approved the final paper.

882

883 **DECLARATION OF INTERESTS**

884 The authors declare that they have no competing interests.

885

886 **FIGURE LEGENDS**

887 **Figure 1. High-light stress-induced anthocyanin biosynthesis is ROS-dependent.**
888 **(A-M),** Pear seedlings were treated with high-light (photon flux density: approximately
889 160 $\mu mol \cdot s^{-1} \cdot m^{-2}$) or high-light supplemented with N, N'-dimethylthiourea (DMTU)
890 treatment. DMTU was applied as ROS scavenger, and pear seedlings under normal light
891 condition were used as Mock (photon flux density: approximately 50 $\mu mol \cdot s^{-1} \cdot m^{-2}$). Pear
892 seedlings were sampled at 0 h, 6 h, 12 h, 24 h, 48 h, 72 h, 96 h. **(A)** Phenotype of pear

893 seedlings (scale bar, 1 cm). **(B)** The anthocyanin contents for pear seedlings (units: A_{530}/g
894 of fresh weight). **(C)** NBT staining for O_2^- in pear seedlings leaves at 0 h, 24 h, 48 h (scale
895 bar, 5 mm). **(D)** Quantification of NBT staining in pear leaves at 0 h, 24 h, 48 h. **(E)** DAB
896 staining for H_2O_2 in pear seedlings leaves at 0 h, 24 h, 48 h (scale bar, 5 mm). **(F)**
897 Quantification of DAB staining in pear leaves at 0 h, 24 h, 48 h. **(G)** The H_2O_2 content for
898 pear seedlings. **(H-M),** The expression levels of *PuCHI*, *PuCHS*, *PuDFR*, *PuF3H*, *PuANS*,
899 *PuMYB10* in pear seedlings under different treatments. *PuACTIN* was amplified as an
900 internal control. Data are presented as means ± s.d. of 3 biological replicates. Asterisks
901 indicate significant differences compared with Mock group **(B)** and **(G-M)**, Mock and High
902 light stress **(D)** and **(F)** (two-tailed Student's *t-test*, $*P < 0.05$, $**P < 0.01$; ns, no
903 significance, $P > 0.05$), all P values are shown in Supplemental Data Set S7.
904
905 **Figure 2. Identification of PuMYB123-like and its interaction with PubHLH3.**
906 **(A)** The expression levels of *PuMYB123-like* in pear seedlings under high-light treatment
907 or high-light supplemented with DMTU treatment. The pear seedlings under normal light
908 condition were used as Mock. *PuACTIN* was amplified as an internal control. **(B)**
909 Phylogenetic analysis of PuMYB123-like. The phylogenetic tree was calculated using the
910 maximum-likelihood method of MEGA X (version 10.1.8). Bootstrap values of 1000
911 replicates for each branch are shown. The protein sequences from pear (Pu, *Pyrus*
912 *ussuriensis*, highlighted with blue dots), apple (Md, *Malus* × *domestica*, highlighted with
913 green dots), Arabidopsis (At, *Arabidopsis thaliana*, highlighted with rose red dots) and
914 strawberry (Fa, *Fragaria* × *ananassa*, highlighted with purple dots). PuMYB123-like
915 (EVM0034726.1) is bolded and enlarged. **(C)** Subcellular localization of PuMYB123-like
916 in *N. benthamiana* leaf cells (scale bar, 25 μm). **(D)** Interaction between PuMYB123-like
917 and PubHLH3 in a yeast two-hybrid assay, with pGADT7-T and pGBKT7-53 as positive
918 controls. DDO, SD/-Trp/-Leu medium; QDO/X/A, SD/-Trp/-Leu/-Ade/-His medium with
919 X-α-gal and Aureobasidin. **(E)** The interaction between PuMYB123-like and PubHLH3
920 was detected by luciferase complementation imaging assays. The pseudocolour scale bar
921 indicates the range of luminescence intensity. **(F)** The interaction between PuMYB123-like
922 and PubHLH3 analyzed using a pull-down assay. PuMYB123-like-His was incubated with

923 GST or PubHLH3-GST. The interaction proteins were precipitated by GST-Trap agarose
924 beads and analyzed by immunoblotting with an anti-GST or anti-His antibody. **(G)** A dual-
925 luciferase assay demonstrated that PuMYB123-like promotes the promoter activity of
926 anthocyanin-related genes (*PuCHS*, *PuANS*, *PuDFR*, *PuUFGT*). The promoter of
927 anthocyanin-related genes was cloned into the pGreenII 0800-LUC (firefly luciferase)
928 vector, and the full-length CDS of *PuMYB123-like* was cloned into the pGreenII 0029 62-
929 SK vector. The empty vector of pGreenII 0029 62-SK was used as control. **(H)** Dual-
930 luciferase assay showed that interaction between PuMYB123-like and PubHLH3
931 significantly enhanced activation of PuMYB123-like on *PuCHS*, *PuDFR* and *PuANS*
932 promoters. Data are presented as means ± s.d. of 3 biological replicates **(A)** or 6 biological
933 replicates **(G)** and **(H)**. Asterisks indicate significant differences compared with Mock **(A)**,
934 empty vector **(G)** or PuMYB123-like **(H)** (two-tailed Student's *t-test*, $*P < 0.05$, $**P <$
935 0.01), all *P* values are shown in Supplemental Data Set S7.
936
937 **Figure 3. PuMYB123-like promotes anthocyanin biosynthesis.**
938 **(A)** Phenotype of pear calli overexpressing or silencing *PuMYB123-like* (scale bar, 1 cm).
939 Wild type pear calli were used as the negative control. Pear calli were incubated under
940 continuous white light at 17°C for 3 d. **(B)** Expression levels of anthocyanin-related genes
941 and *PuMYB123-like* in *PuMYB123-like*-OE *and PuMYB123-like*-RNAi pear calli after
942 light treatment. *PcACTIN* was amplified as an internal control. **(C)** Anthocyanin contents
943 in *PuMYB123-like*-OE and *PuMYB123-like*-RNAi pear calli after light treatment (units:
944 A_{530}/g of fresh weight). **(D)** Phenotype of *Arabidopsis* seedlings ectopic expressing
945 *PuMYB123-like* (scale bar, 2 mm). Wild-type *Arabidopsis* Col-0 was used as the negative
946 control. *Arabidopsis* seedlings were grown on 1/2 MS medium for five days. **(E)** PCR
947 results of wild-type pear calli and *PuMYB123-like* transgenic pear calli lines using
948 transgene-specific primers. *AtPP2A* was amplified as an internal control. **(F)** Anthocyanin
949 contents in transgenic *Arabidopsis* lines (units: A_{530}/g of fresh weight). **(G)** The hypocotyl
950 lengths of transgenic *Arabidopsis* seedlings. **(H)** Expression levels of anthocyanin-related
951 genes in transgenic *Arabidopsis* lines. Data are presented as means ± s.d. of 3 biological
952 replicates **(B)**, **(C)**, **(F)** and **(H)** or 15 biological replicates **(G)**. Asterisks indicate

953 significant differences compared with wild type pear calli **(B)** and **(C)** or wild type
954 *Arabidopsis* **(F-H)**, (two-tailed Student's *t-test*, **P* < 0.05, ***P* < 0.01), all *P* values are
955 shown in Supplemental Data Set S7.
956
957 **Figure 4. Identification of PuHB40 and its response to ROS**.
958 **(A)** The expression pattern of DETs in cluster 14 based on Mfuzz clustering. **(B)** Venn
959 diagram of genes in "purple module" and DETs in cluster 14. **(C)** Numbers of transcription
960 factors in overlapped genes of "purple module" and cluster 14. **(D)** Heat map presenting
961 the expression patterns of transcription factors in overlapped genes of "purple module" and
962 cluster 14 in response to diverse treatments. The values on the right of the heat map indicate
963 the correlation of the expression patterns (FPKMs) between these genes and *PuMYB123-*
964 *like*. **(E)** Distribution of potential binding sites of PuHB40 in *PuMYB123-like* promoter
965 region. Vertical red lines indicate the position of site1 to site4. **(F)** The expression levels of
966 *PuHB40* in pear seedlings under high-light treatment or high-light supplemented with
967 DMTU treatment, and pear seedlings under normal light condition were used as Mock.
968 *PuACTIN* was amplified as an internal control. **(G)** Changes in the PuHB40 abundance in
969 pear seedlings under high-light treatment or high-light supplemented with DMTU
970 treatment for 0 h, 6 h, 24 h, 48 h. The PuHB40 and PuACTIN proteins were detected by
971 immunoblotting with an affinity-purified specific anti-PuHB40 polyclonal antibody and
972 Anti β-Actin monoclonal antibody, respectively. **(H)** Phenotype of pear calli after 4 mM
973 H_2O_2 treatment for two days (scale bar, 1 cm). Pear calli treated with 0 mM H_2O_2 were
974 used as control. **(I)** Anthocyanin contents in pear calli treated with 0 mM or 4 mM H_2O_2
975 for two days (units: A_{530}/g of fresh weight). **(J)** Expression levels of *PcHB40*, *PcMYB123-*
976 *like* and anthocyanin-related genes in pear calli treated with 0 mM or 4 mM H_2O_2 for two
977 days. *PcACTIN* was amplified as an internal control. **(K)** Expression levels of *PcHB40* in
978 pear calli after 0 mM or 4 mM H_2O_2 treatment at 0 h, 3 h, 6 h, 12 h, 24 h, 72 h. *PcACTIN*
979 was amplified as an internal control. **(L)** Subcellular localization of PuHB40 in *N.*
980 *benthamiana* leaf cells (scale bar, 25 μm). Data are presented as means ± s.d. of 3 biological
981 replicates. Asterisks indicate significant differences compared with Mock **(F)** or 0 mM

982 H_2O_2 **(I-K)** (two-tailed Student's *t-test*, **P* < 0.05, ***P* < 0.01), all *P* values are shown in
983 Supplemental Data Set S7.
984
985 **Figure 5. PuHB40 promotes *PuMYB123-like* transcription.**
986 **(A)** Effect of the mutation of potential PuHB40 binding sites on the activation of
987 *PuMYB123-like*. Four potential binding sites (site1 to site4) were mutated into
988 TTTTTTTTT, respectively. The promoters of *PuMYB123-like* with or without potential
989 binding site mutation were cloned into the pGreenII 0800-LUC (firefly luciferase) vector,
990 and the full-length CDS of *PuHB40* was cloned into the pGreenII 0029 62-SK vector. The
991 empty vector of pGreenII 0029 62-SK was used as control. **(B)** The EMSA confirmed that
992 PuHB40 bound to the site4 in the *PuMYB123-like* promoter directly. The *ProPuMYB123-*
993 *like* probe was the biotin-labeled fragment of *PuMYB123-like* promoter containing site4
994 (AAATTATTG), whereas the cold probe was an unlabeled probe (3-, 5-, and 10-fold molar
995 excess). *ProPuMYB123-like*-mut probe was the same as the *ProPuMYB123-like* probe but
996 with site4 (AAATTATTG) mutated to TTTTTTTTT. **(C)** ChIP-qPCR assay results showed
997 the binding of PuHB40 to the *PuMYB123-like* promoter *in vivo*. Cross-linked chromatin
998 samples were extracted from *PuHB40*-MYC overexpressing pear calli with 3 biological
999 replicates and precipitated with an anti-MYC antibody. Eluted DNA was used to amplify
1000 *PuMYB123-like* promoter fragments and eight regions (P1 to P8) were examined, among
1001 which P6 containing site4. Pear calli overexpressing the *MYC* sequence were used as a
1002 negative control. Three biological replicates of pear calli were used in the ChIP assay. **(D)**
1003 Transient overexpression of *PuHB40* with or without transient silencing of *PuMYB123-*
1004 *like* in pear seedlings. The full-length CDS of *PuHB40* and reverse complementary gene
1005 fragment (~200 to 300 bp) of *PuMYB123-like* were inserted into the pCAMBIA1301 vector
1006 under the control of the 35S promoter. The plasmids were transformed into *A. tumefaciens*
1007 GV3101 and infiltrated into pear seedlings by vacuum. The infiltrated pear seedlings were
1008 firstly incubated in darkness for two days and then exposed to continuous white light for
1009 three days. Pear seedlings infiltrated with an empty pCAMBIA1301 vector were used as a
1010 control. **(E)** Anthocyanin contents in pear seedlings (units: A_{530}/g of fresh weight). **(F)**
1011 Expression levels of *PuHB40*, *PuMYB123-like* and anthocyanin-related genes in pear

1012 seedlings. Data are presented as means ± s.d. of 3 biological replicates **(C), (E)** and **(F)** or
1013 6 biological replicates **(A)**. Asterisks indicate significant differences compared with empty
1014 vector **(A)** or control **(C), (E)** and **(F)** (two-tailed Student's *t-test*, **P* < 0.05, ***P* < 0.01;
1015 ns, no significance, *P* > 0.05), all *P* values are shown in Supplemental Data Set S7.
1016
1017 **Figure 6. PuHB40 promotes anthocyanin biosynthesis.**
1018 **(A)** Phenotype of pear calli overexpressing and silencing *PuHB40* (scale bar, 1 cm). Wild
1019 type pear calli were used as the negative control. Pear calli were incubated under
1020 continuous white light at 17°C for 3 d. **(B)** Expression levels of *PuHB40* in *PuHB40*-OE
1021 and *PuHB40*-RNAi pear calli after light treatment. *PcACTIN* was amplified as an internal
1022 control. **(C)** Anthocyanin contents in *PuHB40*-OE and *PuHB40*-RNAi pear calli after light
1023 treatment (units: A_{530}/g of fresh weight). **(D)** Expression levels of *PcMYB123-like* and
1024 anthocyanin-related genes in *PuHB40*-OE and *PuHB40*-RNAi pear calli after light
1025 treatment. *PcACTIN* was amplified as an internal control. **(E)** Phenotype of *Arabidopsis*
1026 seedlings ectopic expressing *PuHB40* (scale bar, 2 mm). Wild-type *Arabidopsis* Col-0 was
1027 used as the negative control. *Arabidopsis* seedlings were grown on 1/2 MS medium for
1028 five days. **(F)** PCR results of wild-type pear calli and *PuHB40* transgenic pear calli lines
1029 using transgene-specific primers. *AtPP2A* was amplified as an internal control. **(G)**
1030 Anthocyanin contents in transgenic *Arabidopsis* lines (units: A_{530}/g of fresh weight). **(H)**
1031 The hypocotyl lengths of transgenic *Arabidopsis* seedlings (units: A_{530}/g of fresh weight).
1032 **(I)** Expression levels of anthocyanin-related genes in transgenic *Arabidopsis* lines. Data
1033 are presented as means ± s.d. of 3 biological replicates **(B-D)**, **(G)** and **(I)** or 15 biological
1034 replicates **(H)**. Asterisks indicate significant differences compared with wild type pear calli
1035 **(B-D)** or wild type *Arabidopsis* **(G-I)** (two-tailed Student's *t-test*, **P* < 0.05, ***P* < 0.01),
1036 all *P* values are shown in Supplemental Data Set S7.
1037
1038 **Figure 7. Identification of PuPP2AA2 and its interaction with PuHB40.**
1039 **(A)** Phylogenetic analysis of PuPP2AA2. The phylogenetic tree was calculated using the
1040 maximum-likelihood method of MEGA X (version 10.1.8). Bootstrap values of 1000
1041 replicates for each branch are shown. The protein sequences from pear (Pu, *Pyrus*

1042 *ussuriensis*, highlighted with blue dots) and Arabidopsis (*Arabidopsis thaliana*, highlighted
1043 with rose red dots). PuPP2AA2 (EVM0003533.1) is bolded and enlarged. **(B)** Subcellular
1044 localization of PuPP2AA2 in *N. benthamiana* leaf cells (scale bar, 25 μm). **(C)** The
1045 expression levels of *PuPP2AA2* in pear seedlings under high-light treatment or high-light
1046 supplemented with DMTU treatment. *PuACTIN* was amplified as an internal control. **(D)**
1047 Changes in the PuPP2AA2 abundance in pear seedlings. Pear seedlings with the transient
1048 overexpression of MYC-tagged *PuPP2AA2* were exposed to high-light treatment or high-
1049 light supplemented with DMTU treatment for 0 h, 3 h, 6 h, 12 h. The PuPP2AA2 and
1050 PuACTIN proteins were detected by immunoblotting with anti-MYC monoclonal antibody
1051 and Anti β-Actin monoclonal antibody, respectively. **(E)** The interaction between
1052 PuPP2AA2 and PuHB40 using the pull-down assay. PuHB40-His was incubated with GST
1053 or PuPP2AA2-GST. The interactive proteins were precipitated by GST-Trap agarose beads
1054 and analyzed by immunoblotting with an anti-GST or anti-His antibody. **(F)** The interaction
1055 between PuPP2AA2 and PuHB40 was detected by luciferase complementation imaging
1056 assays. The pseudocolour scale bar indicates the range of luminescence intensity. **(G)**
1057 Physical association between PuPP2AA2 and PuHB40 confirmed by a BiFC assay.
1058 Fluorescence indicates positive interactions (scale bar, 25 μm). Data are presented as means
1059 ± s.d. of 3 biological replicates. Asterisks indicate significant differences compared with
1060 high-light stress supplemented with DMTU treatment (two-tailed Student's *t-test*, $*P <$
1061 0.05), all P values are shown in Supplemental Data Set S7.
1062
1063 **Figure 8. PuHB40 was dephosphorylated by PP2A phosphatase.**
1064 **(A)** Phos-tag analysis of phosphorylation of PuHB40 after cantharidin treatment. *A.*
1065 *tumefaciens* GV3101 containing PuHB40-GFP plasmid was infiltrated into *N.*
1066 *benthamiana* leaves by injection and 50 μM cantharidin was injected into the same position
1067 as the agrobacteria after 24 h. *N. benthamiana* leaves injected with DMSO of
1068 corresponding concentration were used as negative control. Protein samples were extracted
1069 from *N. benthamiana* leaves after 24 h and were separated in a Phos-tag gel (upper panel),
1070 and PuHB40-GFP with different phosphorylated status was detected using the anti-GFP
1071 antibody. Total PuHB40-GFP proteins were also analyzed by SDS-PAGE without Phos-tag

1072 (indicated as “Regular”), and were detected using anti-GFP antibody (lower panel). P+ and
1073 P- indicate phosphorylated and non-phosphorylated form of PuHB40, respectively. The
1074 intensity of the bands was measured with the Image J software and the ratio of P+/P− bands
1075 was calculated. **(B)** Immunoblotting analysis showing that the PP2A complex directly
1076 dephosphorylates PuHB40 *in vitro*. MYC, PP2A complex, and PuHB40-GFP were
1077 immunopurified from pear seedlings transiently overexpressing MYC, PuPP2AA2-MYC,
1078 and PuHB40-GFP using MYC-Trap or GFP-Trap, respectively. After incubation of PP2A
1079 complexes with PuHB40-GFP (MYC with PuHB40-GFP was set as control), protein
1080 samples in the reaction system were separated in Phos-tag gel (upper panel) and detected
1081 using the anti-PuHB40 antibody. The intensity of the bands was measured with the Image
1082 J software and the ratio of P+/P− bands was calculated Total proteins in the reaction system
1083 were analyzed by SDS-PAGE without Phos-tag (indicated as “Regular”). PuHB40-GFP,
1084 MYC and PuPP2AA2-MYC were set as the loading controls and detected by the anti-
1085 PuHB40 (middle panel) or anti-MYC (lower panel) antibody, respectively. **(C)** Subcellular
1086 localization of PuPP2AA2D in *N. benthamiana* leaf cells (scale bar, 25 μm). PuPP2AA2D
1087 is PuPP2AA2 with the deletion of heat repeats 14 and 15 in the C-terminal. **(D)** The
1088 interaction between PuPP2AA2D and PuHB40 confirmed by a BiFC assay. Fluorescence
1089 indicates positive interactions (scale bar, 25 μm). **(E)** The interaction between PuPP2AA2D
1090 and PuHB40 was detected by luciferase complementation imaging assays. The
1091 pseudocolour scale bar indicates the range of luminescence intensity. **(F)** Immunoblotting
1092 analysis showing that PP2A dephosphorylates PuHB40 *in vivo*. Protein extracts from *N.*
1093 *benthamiana* leaves co-infiltrated PuHB40-GFP with MYC, PuPP2AA2-MYC, or
1094 PuPP2AA2D-MYC were separated in Phos-tag gel (upper panel) and detected using the
1095 anti-GFP antibody (MYC with PuHB40-GFP was set as control). The intensity of the bands
1096 was measured with the Image J software and the ratio of P+/P− bands was calculated. Total
1097 PuHB40-GFP, MYC, PuPP2AA2-MYC and PuPP2AA2D-MYC proteins were also
1098 analyzed by SDS-PAGE without Phos-tag (indicated as “Regular”). PuHB40-GFP, MYC,
1099 PuPP2AA2-MYC and PuPP2AA2D-MYC were set as the loading controls and detected
1100 by the anti-GFP (middle panel) or anti-MYC (lower panel) antibody, respectively. **(G)**
1101 Dual-luciferase assay showed that dephosphorylation of PuHB40 by PP2A significantly

1102 inhibited the activation of *PuMYB123-like* promoter by PuHB40. The *PuMYB123-like*
1103 promoter was cloned into the pGreenII 0800-LUC (firefly luciferase) vector, and the full-
1104 length CDS of *PuHB40*, *PuPP2AA2* and *PuPP2AA2D* were cloned into the pGreenII 0029
1105 62-SK vector. The PuHB40 was used as control. Data are presented as means ± s.d. of 6
1106 biological replicates **(G)**. Asterisks indicate significant differences compared PuHB40 **(G)**
1107 (two-tailed Student's *t-test*, $^{**}P < 0.01$; ns, no significance, $P > 0.05$), all P values are
1108 shown in Supplemental Data Set S7.
1109
1110 **Figure 9. Attenuation of PuHB40-induced anthocyanin biosynthesis by PuPP2AA2**.
1111 **(A)** Phenotype of pear calli overexpressing *PuPP2AA2* (scale bar, 1 cm). Wild type pear
1112 calli were used as the negative control. Pear calli were incubated under continuous white
1113 light at 17°C for 3 d. **(B)** Anthocyanin contents in *PuPP2AA2*-OE after light treatment
1114 (units: A_{530}/g of fresh weight). **(C)** Expression levels of *PuPP2AA2* and anthocyanin-
1115 related genes in *PuPP2AA2*-OE pear calli after light treatment. *PcACTIN* was amplified as
1116 an internal control. **(D)** Transient overexpression of *PuHB40* with or without transient
1117 overexpressing of *PuPP2AA2* in pear seedlings. The full-length CDS of *PuHB40* and
1118 *PuPP2AA2* were inserted into the pCAMBIA1301 vector under the control of the 35S
1119 promoter. The plasmids were transformed into *A. tumefaciens* GV3101 and infiltrated into
1120 pear seedlings by vacuum. The infiltrated pear seedlings were firstly incubated in darkness
1121 for two days and then exposed to continuous white light for three days. Pear seedlings
1122 infiltrated with an empty pCAMBIA1301 vector were used as a control. **(E)** Anthocyanin
1123 contents in pear seedlings (units: A_{530}/g of fresh weight). **(F)** Expression levels of *PuHB40*,
1124 *PuPP2AA2*, *PuMYB123-like* and anthocyanin-related genes in pear seedlings. **(G)**
1125 Transient overexpression of *PuHB40* with or without transient overexpressing of
1126 *PuPP2AA2* in pear fruits (scale bar, 1 cm). The full-length CDS of *PuHB40* and *PuPP2AA2*
1127 were cloned to the pGreenII 0029 62-SK vector under the control of the 35S promoter. Pear
1128 fruits were infiltrated with *A. tumefaciens* GV3101 cells containing the recombinant
1129 plasmid using a needle syringe. Fruits infiltrated with an empty pGreenII 0029 62-SK
1130 vector were used as a control. The phenotypes were examined after dark treatment for one
1131 day followed by the light treatment for four days **(H)** Total anthocyanin contents in pear

1132 fruits (units: A_{530}/g of fresh weight). **(I)** Expression levels of *PuHB40*, *PuPP2AA2* and
1133 anthocyanin-related genes in pear fruits. Data are presented as means ± s.d. of 3 biological
1134 replicates. Asterisks indicate significant differences compared with wild type pear calli **(B)**
1135 and **(C)** or empty vector **(E), (F), (H)** and **(I)** (two-tailed Student's *t-test*, $*P < 0.05$, $**P <$
1136 0.01; ns, no significance, $P > 0.05$), all P values are shown in Supplemental Data Set S7.
1137

1138 **Figure 10. Proposed model for PuHB40-mediated ROS-dependent anthocyanin**
1139 **biosynthesis in pears.**

1140 PuHB40 is the key transcription factor in ROS-induced anthocyanin biosynthesis. ROS
1141 promote PuHB40 expression and then positively regulate its transcriptional activity on
1142 PuMYB123-like/PubHLH3 complex to induce anthocyanin biosynthesis. The
1143 transcriptional activity of PuHB40 depends on its phosphorylation level which is regulated
1144 by PP2A. ROS maintain phosphorylation of PuHB40 at a high level, and enhance the
1145 transcriptional activity of PuHB40 on *PuMYB123-like* by suppressing the transcription of
1146 *PuPP2AA2* under high-light stress, and thus promote anthocyanin biosynthesis.
1147

1148 **REFERENCES**

1149 **Acero N, Gradillas A, Beltran M, Garcia A, Munoz Mingarro D.** Comparison of
1150 phenolic compounds profile and antioxidant properties of different sweet cherry
1151 (*Prunus avium* L.) varieties. Food Chemistry. 2019:**279**:260-271.
1152 https://doi.org/10.1016/j.foodchem.2018.12.008

1153 **Altangerel N, Ariunbold GO, Gorman C, Alkahtani MH, Borrego EJ, Bohlmeyer D,**
1154 **Hemmer P, Kolomiets MV, Yuan JS, Scully MO.** In vivo diagnostics of early
1155 abiotic plant stress response via Raman spectroscopy. Proceedings of the National
1156 Academy of Sciences of the United States of America. 2017:**114**(13):3393-3396.
1157 https://doi.org/10.1073/pnas.1701328114

1158 **An JP, Wang XF, Zhang XW, Xu HF, Bi SQ, You CX, Hao YJ.** An apple MYB
1159 transcription factor regulates cold tolerance and anthocyanin accumulation and
1160 undergoes MIEL1-mediated degradation. Plant Biotechnology Journal.
1161 2020:**18**(2):337-353. https://doi.org/10.1111/pbi.13201

1162 **An XH, Tian Y, Chen KQ, Liu XJ, Liu DD, Xie XB, Cheng CG, Cong PH, Hao YJ.**
1163 MdMYB9 and MdMYB11 are involved in the regulation of the JA-induced
1164 biosynthesis of anthocyanin and proanthocyanidin in apples. Plant and Cell
1165 Physiology. 2015:**56**(4):650-662. https://doi.org/10.1093/pcp/pcu205
1166 **Ariel FD, Manavella PA, Dezar CA, Chan RL.** The true story of the HD-Zip family.
1167 Trends in Plant Science. 2007:**12**(9):419-426.
1168 https://doi.org/10.1016/j.tplants.2007.08.003
1169 **Asada K.** Production and scavenging of reactive oxygen species in chloroplasts and their
1170 functions. Plant Physiology. 2006:**141**(2):391-396.
1171 https://doi.org/10.1104/pp.106.082040
1172 **Bai S, Tao R, Yin L, Ni J, Yang Q, Yan X, Yang F, Guo X, Li H, Teng Y.** Two B-box
1173 proteins, PpBBX18 and PpBBX21, antagonistically regulate anthocyanin
1174 biosynthesis via competitive association with *Pyrus pyrifolia* ELONGATED
1175 HYPOCOTYL 5 in the peel of pear fruit. Plant Journal. 2019a:**100**(6):1208-1223.
1176 https://doi.org/10.1111/tpj.14510
1177 **Bai S, Tao R, Tang Y, Yin L, Ma Y, Ni J, Yan X, Yang Q, Wu Z, Zeng Y, et al.** BBX16,
1178 a B-box protein, positively regulates light-induced anthocyanin accumulation by
1179 activating *MYB10* in red pear. Plant Biotechnology Journal. 2019b:**17**(10):1985-
1180 1997. https://doi.org/10.1111/pbi.13114
1181 **Baudry A, Heim MA, Dubreucq B, Caboche M, Weisshaar B, Lepiniec L.** TT2, TT8,
1182 and TTG1 synergistically specify the expression of *BANYULS* and
1183 proanthocyanidin biosynthesis in *Arabidopsis thaliana*. Plant Journal.
1184 2004:**39**(3):366-380. https://doi.org/10.1111/j.1365-313X.2004.02138.x
1185 **Bi X, Zhang J, Chen C, Zhang D, Li P, Ma F.** Anthocyanin contributes more to hydrogen
1186 peroxide scavenging than other phenolics in apple peel. Food Chemistry.
1187 2014:**152**:205-209. https://doi.org/10.1016/j.foodchem.2013.11.088
1188 **Bian C, Guo X, Zhang Y, Wang L, Xu T, DeLong A, Dong J.** Protein phosphatase 2A
1189 promotes stomatal development by stabilizing SPEECHLESS in *Arabidopsis*.
1190 Proceedings of the National Academy of Sciences of the United States of America.
1191 2020:**117**(23):13127-13137. https://doi.org/10.1073/pnas.1912075117

1192 **Byrne DP, Shrestha S, Galler M, Cao M, Daly LA, Campbell AE, Eyers CE, Veal EA,**
1193 **Kannan N, Eyers PA.** Aurora A regulation by reversible cysteine oxidation reveals
1194 evolutionarily conserved redox control of Ser/Thr protein kinase activity. Science
1195 Signaling. 2020:**13**(613). https://doi.org/10.1126/scisignal.aax2713
1196 **Catalá R, Medina J, Salinas J.** Integration of low temperature and light signaling during
1197 cold acclimation response in *Arabidopsis*. Proceedings of the National Academy of
1198 Sciences of the United States of America. 2011:**108**(39):16475-16480.
1199 https://doi.org/10.1073/pnas.1107161108
1200 **Chan KX, Mabbitt PD, Phua SY, Mueller JW, Nisar N, Gigolashvili T, Stroeher E,**
1201 **Grassl J, Arlt W, Estavillo GM, et al.** Sensing and signaling of oxidative stress in
1202 chloroplasts by inactivation of the SAL1 phosphoadenosine phosphatase.
1203 Proceedings of the National Academy of Sciences of the United States of America.
1204 2016:**113**(31):E4567-4576. https://doi.org/10.1073/pnas.1604936113
1205 **Chen C, Wu Y, Li J, Wang X, Zeng Z, Xu J, Liu Y, Feng J, Chen H, He Y, et al.** TBtools-
1206 II: A "one for all, all for one" bioinformatics platform for biological big-data mining.
1207 Molecular Plant. 2023:**16**(11):1733-1742.
1208 https://doi.org/10.1016/j.molp.2023.09.010
1209 **Choi S, Kwon YR, Hossain MA, Hong S-W, Lee B-h, Lee H.** A mutation in *ELA1*, an
1210 age-dependent negative regulator of *PAP1/MYB75*, causes UV- and cold stress-
1211 tolerance in *Arabidopsis thaliana* seedlings. Plant Science. 2009:**176**(5):678-686.
1212 https://doi.org/10.1016/j.plantsci.2009.02.010
1213 **Croce R, van Amerongen H.** Natural strategies for photosynthetic light harvesting. Nature
1214 Chemical Biology. 2014:**10**(7):492-501. https://doi.org/10.1038/nchembio.1555
1215 **Curtis W, Muldrow M, Parker N, Barkley R.** *N,N'*-dimethylthiourea dioxide formation
1216 from *N,N'*-dimethylthiourea reflects hydrogen-peroxide concentrations in simple
1217 biological-systems. Proceedings of the National Academy of Sciences of the United
1218 States of America. 1988:**85**(10):3422-3425.
1219 https://doi.org/10.1073/pnas.85.10.3422
1220 **Das PK, Shin DH, Choi SB, Yoo SD, Choi G, Park YI.** Cytokinins enhance sugar-
1221 induced anthocyanin biosynthesis in Arabidopsis. Molecules and Cells.

1222 2012:**34**(1):93-101. https://doi.org/10.1007/s10059-012-0114-2
1223 **DeLong A.** Switching the flip: protein phosphatase roles in signaling pathways. Current
1224 Opinion in Plant Biology. 2006:**9**(5):470-477.
1225 https://doi.org/10.1016/j.pbi.2006.07.015
1226 **Deng J, Sun W, Zhang B, Sun S, Xia L, Miao Y, He L, Lindsey K, Yang X, Zhang X.**
1227 GhTCE1-GhTCEE1 dimers regulate transcriptional reprogramming during wound-
1228 induced callus formation in cotton. Plant Cell. 2022:**34**(11):4554-4568.
1229 https://doi.org/10.1093/plcell/koac252
1230 **Dubos C, Stracke R, Grotewold E, Weisshaar B, Martin C, Lepiniec L.** MYB
1231 transcription factors in *Arabidopsis*. Trends in Plant Science. 2010:**15**(10):573-581.
1232 https://doi.org/10.1016/j.tplants.2010.06.005
1233 **Durian G, Rahikainen M, Alegre S, Brosche M, Kangasjarvi S.** Protein phosphatase 2A
1234 in the regulatory network underlying biotic stress resistance in plants. Frontiers in
1235 Plant Science. 2016:**7**:812. https://doi.org/10.3389/fpls.2016.00812
1236 **Espley RV, Hellens RP, Putterill J, Stevenson DE, Kutty-Amma S, Allan AC.** Red
1237 colouration in apple fruit is due to the activity of the MYB transcription factor,
1238 MdMYB10. Plant Journal. 2007:**49**(3):414-427. https://doi.org/10.1111/j.1365-
1239 313X.2006.02964.x
1240 **Farkas I, Dombradi V, Miskei M, Szabados L, Koncz C.** *Arabidopsis* PPP family of
1241 serine/threonine phosphatases. Trends in Plant Science. 2007:**12**(4):169-176.
1242 https://doi.org/10.1016/j.tplants.2007.03.003
1243 **Feng S, Wang Y, Yang S, Xu Y, Chen X.** Anthocyanin biosynthesis in pears is regulated
1244 by a R2R3-MYB transcription factor PyMYB10. Planta. 2010:**232**(1):245-255.
1245 https://doi.org/10.1007/s00425-010-1170-5
1246 **Foyer CH, Noctor G.** Redox regulation in photosynthetic organisms: signaling,
1247 acclimation, and practical implications. Antioxidants & Redox Signaling.
1248 2009:**11**(4):861-905. https://doi.org/10.1089/ars.2008.2177
1249 **Galvez-Valdivieso G, Fryer MJ, Lawson T, Slattery K, Truman W, Smirnoff N, Asami**
1250 **T, Davies WJ, Jones AM, Baker NR, et al.** The high light response in *Arabidopsis*
1251 involves ABA signaling between vascular and bundle sheath cells. Plant Cell.

1252 2009:**21**(7):2143-2162. https://doi.org/10.1105/tpc.108.061507
1253 **Gao Y, Yang Q, Yan X, Wu X, Yang F, Li J, Wei J, Ni J, Ahmad M, Bai S, et al.** High-
1254 quality genome assembly of 'Cuiguan' pear (*Pyrus pyrifolia*) as a reference genome
1255 for identifying regulatory genes and epigenetic modifications responsible for bud
1256 dormancy. Horticulture Research. 2021:**8**(1):197. https://doi.org/10.1038/s41438-
1257 021-00632-w
1258 **Gould KS, McKelvie J, Markham KR.** Do anthocyanins function as antioxidants in
1259 leaves? Imaging of H_2O_2 in red and green leaves after mechanical injury. Plant Cell
1260 and Environment. 2002:**25**(10):1261-1269. https://doi.org/10.1046/j.1365-
1261 3040.2002.00905.x
1262 **Groves MR, Hanlon N, Turowski P, Hemmings BA, Barford D.** The structure of the
1263 protein phosphatase 2A PR65/A subunit reveals the conformation of its 15
1264 tandemly repeated HEAT motifs. Cell. 1999:**96**(1):99-110.
1265 https://doi.org/10.1016/S0092-8674(00)80963-0
1266 **Gupta R, Luan S.** Redox control of protein tyrosine phosphatases and mitogen-activated
1267 protein kinases in plants. Plant Physiology. 2003:**132**(3):1149-1152.
1268 https://doi.org/10.1104/pp.103.020792
1269 **Harris JC, Hrmova M, Lopato S, Langridge P.** Modulation of plant growth by HD-Zip
1270 class I and II transcription factors in response to environmental stimuli. New
1271 Phytologist. 2011:**190**(4):823-837. https://doi.org/10.1111/j.1469-
1272 8137.2011.03733.x
1273 **Himmelbach A, Hoffmann T, Leube M, Hohener B, Grill E.** Homeodomain protein
1274 ATHB6 is a target of the protein phosphatase ABI1 and regulates hormone
1275 responses in *Arabidopsis*. EMBO Journal. 2002:**21**(12):3029-3038.
1276 https://doi.org/10.1093/emboj/cdf316
1277 **Hipsch M, Lampl N, Zelinger E, Barda O, Waiger D, Rosenwasser S.** Sensing stress
1278 responses in potato with whole-plant redox imaging. Plant Physiology.
1279 2021:**187**(2):618-631. https://doi.org/10.1093/plphys/kiab159
1280 **Honkanen RE.** Cantharidin, another natural toxin that inhibits the activity of
1281 serine/threonine protein phosphatases types 1 and 2A. FEBS Letters.

1993:**330**(3):283-286. https://doi.org/10.1016/0014-5793(93)80889-3

Hu CD, Chinenov Y, Kerppola TK. Visualization of interactions among bZip and Rel family proteins in living cells using bimolecular fluorescence complementation. Molecular Cell. 2002:**9**(4):789-798. https://doi.org/10.1016/S1097-2765(02)00496-3

Jaakola L. New insights into the regulation of anthocyanin biosynthesis in fruits. Trends in Plant Science. 2013:**18**(9):477-483. https://doi.org/10.1016/j.tplants.2013.06.003

Jalmi SK, Sinha AK. ROS mediated MAPK signaling in abiotic and biotic stress- striking similarities and differences. Frontiers in Plant Science. 2015:**6**:769. https://doi.org/10.3389/fpls.2015.00769

Janssens V, Goris J. Protein phosphatase 2A: a highly regulated family of serine/threonine phosphatases implicated in cell growth and signalling. Biochemical Journal. 2001:**353**(3):417-439. https://doi.org/10.1042/0264-6021:3530417

Jia M, Li X, Wang W, Li T, Dai Z, Chen Y, Zhang K, Zhu H, Mao W, Feng Q, et al. SnRK2 subfamily I protein kinases regulate ethylene biosynthesis by phosphorylating HB transcription factors to induce *ACO1* expression in apple. New Phytologist. 2022:**234**(4):1262-1277. https://doi.org/10.1111/nph.18040

Jiang T, He Y, Wu Z, Cui Y, Wang X, Huang H, Fan Y, Han M, Wang J, Wang S, et al. Enhancing stimulation of cyaniding, *GhLDOX3* activates reactive oxygen species to regulate tolerance of alkalinity negatively in cotton. Ecotoxicology and Environmental Safety. 2023:**267**:115655. https://doi.org/10.1016/j.ecoenv.2023.115655

Kamibayashi C, Lickteig RL, Estes R, Walter G, Mumby MC. Expression of the A subunit of protein phosphatase 2A and characterization of its interactions with the catalytic and regulatory subunits. Journal of Biological Chemistry. 1992:**267**(30):21864-21872. https://doi.org/10.1016/s0021-9258(19)36692-x

Kerchev P, Waszczak C, Lewandowska A, Willems P, Shapiguzov A, Li Z, Alseekh S, Muhlenbock P, Hoeberichts FA, Huang J, et al. Lack of GLYCOLATE OXIDASE1, but not GLYCOLATEOXIDASE2, attenuates the photorespiratory

1312 phenotype of CATALASE2-deficient Arabidopsis. Plant Physiology.
1313 2016:**171**(3):1704-1719. https://doi.org/10.1104/pp.16.00359
1314 **Kovtun Y, Chiu WL, Tena G, Sheen J.** Functional analysis of oxidative stress-activated
1315 mitogen-activated protein kinase cascade in plants. Proceedings of the National
1316 Academy of Sciences of the United States of America. 2000:**97**(6):2940-2945.
1317 https://doi.org/10.1073/pnas.97.6.2940
1318 **Kumar S, Stecher G, Li M, Knyaz C, Tamura K.** MEGA X: Molecular Evolutionary
1319 Genetics Analysis across Computing Platforms. Molecular Biology and Evolution.
1320 2018:**35**(6):1547-1549. https://doi.org/10.1093/molbev/msy096
1321 **Landi M, Tattini M, Gould KS.** Multiple functional roles of anthocyanins in plant-
1322 environment interactions. Environmental and Experimental Botany. 2015:**119**:4-17.
1323 https://doi.org/10.1016/j.envexpbot.2015.05.012
1324 **Lee DW, Gould KS.** Why leaves turn red: pigments called anthocyanins probably protect
1325 leaves from light damage by direct shielding and by scavenging free radicals.
1326 American Scientist. 2002:**90**(6):524-531. https://doi.org/10.1511/2002.6.524
1327 **Lesk C, Rowhani P, Ramankutty N.** Influence of extreme weather disasters on global
1328 crop production. Nature. 2016:**529**(7584):84-87.
1329 https://doi.org/10.1038/nature16467
1330 **Li Y, Wang Y, Tan S, Li Z, Yuan Z, Glanc M, Domjan D, Wang K, Xuan W, Guo Y, et**
1331 **al.** Root growth adaptation is mediated by PYLs ABA receptor-PP2A protein
1332 phosphatase complex. Advanced Science. 2020:**7**(3):1901455.
1333 https://doi.org/10.1002/advs.201901455
1334 **Li YY, Mao K, Zhao C, Zhao XY, Zhang HL, Shu HR, Hao YJ.** MdCOP1 ubiquitin E3
1335 ligases interact with MdMYB1 to regulate light-induced anthocyanin biosynthesis
1336 and red fruit coloration in apple. Plant Physiology. 2012:**160**(2):1011-1022.
1337 https://doi.org/10.1104/pp.112.199703
1338 **Li Z, Wakao S, Fischer BB, Niyogi KK.** Sensing and responding to excess light. Annual
1339 Review of Plant Biology. 2009:**60**:239-260.
1340 https://doi.org/10.1146/annurev.arplant.58.032806.103844
1341 **Lillo C, Kataya AR, Heidari B, Creighton MT, Nemie-Feyissa D, Ginbot Z, Jonassen**

1342 **EM.** Protein phosphatases PP2A, PP4 and PP6: mediators and regulators in
1343 development and responses to environmental cues. Plant Cell and Environment.
1344 2014:**37**(12):2631-2648. https://doi.org/10.1111/pce.12364
1345 **Lin-Wang K, Micheletti D, Palmer J, Volz R, Lozano L, Espley R, Hellens RP, Chagne**
1346 **D, Rowan DD, Troggio M, et al.** High temperature reduces apple fruit colour via
1347 modulation of the anthocyanin regulatory complex. Plant Cell and Environment.
1348 2011:**34**(7):1176-1190. https://doi.org/10.1111/j.1365-3040.2011.02316.x
1349 **Liu W, Feng Y, Yu S, Fan Z, Li X, Li J, Yin H.** The flavonoid biosynthesis network in
1350 plants. International Journal of Molecular Sciences. 2021:**22**(23).
1351 https://doi.org/10.3390/ijms222312824
1352 **Livak KJ, Schmittgen TD.** Analysis of relative gene expression data using real-time
1353 quantitative PCR and the $2^{-\triangle\triangle CT}$ method. Methods. 2001:**25**(4):402-408.
1354 https://doi.org/10.1006/meth.2001.1262
1355 **Mine A, Berens ML, Nobori T, Anver S, Fukumoto K, Winkelmuller TM, Takeda A,**
1356 **Becker D, Tsuda K.** Pathogen exploitation of an abscisic acid- and jasmonate-
1357 inducible MAPK phosphatase and its interception by *Arabidopsis* immunity.
1358 Proceedings of the National Academy of Sciences of the United States of America.
1359 2017:**114**(28):7456-7461. https://doi.org/10.1073/pnas.1702613114
1360 **Mittler R.** ROS are good. Trends in Plant Science. 2017:**22**(1):11-19.
1361 https://doi.org/10.1016/j.tplants.2016.08.002
1362 **Mittler R, Zandalinas SI, Fichman Y, Van Breusegem F.** Reactive oxygen species
1363 signalling in plant stress responses. Nature Reviews Molecular Cell Biology.
1364 2022:**23**(10):663-679. https://doi.org/10.1038/s41580-022-00499-2
1365 **Mullineaux PM, Exposito-Rodriguez M, Laissue PP, Smirnoff N.** ROS-dependent
1366 signalling pathways in plants and algae exposed to high light: Comparisons with
1367 other eukaryotes. Free Radical Biology And Medicine. 2018:**122**:52-64.
1368 https://doi.org/10.1016/j.freeradbiomed.2018.01.033
1369 **Naing AH, Kim CK.** Roles of R2R3-MYB transcription factors in transcriptional
1370 regulation of anthocyanin biosynthesis in horticultural plants. Plant Molecular
1371 Biology. 2018:**98**(1-2):1-18. https://doi.org/10.1007/s11103-018-0771-4

1372 **Nakabayashi R, Yonekura-Sakakibara K, Urano K, Suzuki M, Yamada Y, Nishizawa**
1373 **T, Matsuda F, Kojima M, Sakakibara H, Shinozaki K, et al.** Enhancement of
1374 oxidative and drought tolerance in Arabidopsis by overaccumulation of antioxidant
1375 flavonoids. Plant Journal. 2014:**77**(3):367-379. https://doi.org/10.1111/tpj.12388
1376 **Neill SO, Gould KS, Kilmartin PA, Mitchell KA, Markham KR.** Antioxidant activities
1377 of red versus green leaves in *Elatostema rugosum*. Plant Cell and Environment.
1378 2002:**25**(4):539-547. https://doi.org/10.1046/j.1365-3040.2002.00837.x
1379 **Ni J, Premathilake AT, Gao Y, Yu W, Tao R, Teng Y, Bai S.** Ethylene-activated
1380 PpERF105 induces the expression of the repressor-type R2R3-MYB gene
1381 *PpMYB140* to inhibit anthocyanin biosynthesis in red pear fruit. Plant Journal.
1382 2021:**105**(1):167-181. https://doi.org/10.1111/tpj.15049
1383 **Ni J, Wang S, Yu W, Liao Y, Pan C, Zhang M, Tao R, Wei J, Gao Y, Wang D, et al.** The
1384 ethylene-responsive transcription factor PpERF9 represses *PpRAP2.4* and
1385 *PpMYB114* via histone deacetylation to inhibit anthocyanin biosynthesis in pear.
1386 Plant Cell. 2023:**35**(6):2271-2292. https://doi.org/10.1093/plcell/koad077
1387 **Ni L, Fu X, Zhang H, Li X, Cai X, Zhang P, Liu L, Wang Q, Sun M, Wang QW, et al.**
1388 Abscisic Acid Inhibits Rice Protein Phosphatase PP45 via H_2O_2 and Relieves
1389 Repression of the Ca^{2+}/CaM-Dependent Protein Kinase DMI3. Plant Cell.
1390 2019:**31**(1):128-152. https://doi.org/10.1105/tpc.18.00506
1391 **Olsson AS, Engström P, Söderman E.** The homeobox genes *ATHB12* and *ATHB7* encode
1392 potential regulators of growth in response to water deficit in *Arabidopsis*. Plant
1393 Molecular Biology. 2004:**55**(5):663-677. https://doi.org/10.1007/s11103-004-
1394 1581-4
1395 **Pratyusha DS, Sarada DVL.** MYB transcription factors-master regulators of
1396 phenylpropanoid biosynthesis and diverse developmental and stress responses.
1397 Plant Cell Reports. 2022:**41**(12):2245-2260. https://doi.org/10.1007/s00299-022-
1398 02927-1
1399 **Qu Y, Bai X, Zhu YJ, Qi R, Tian G, Wang Y, Li YH, Zhang KM.** Reactive Oxygen
1400 Species Acts as an Important Inducer in Low-temperature-induced Anthocyanin
1401 Biosynthesis in *Begonia semperflorens*. Journal of the American Society for

1402 Horticultural Science. 2018:**143**(6):486-493.
1403 https://doi.org/10.21273/JASHS04488-18
1404 **Ren H, Rao J, Tang M, Li Y, Dang X, Lin D.** PP2A interacts with KATANIN to promote
1405 microtubule organization and conical cell morphogenesis. Journal of Integrative
1406 Plant Biology. 2022:**64**(8):1514-1530. https://doi.org/10.1111/jipb.13281
1407 **Ruediger R, Hentz M, Fait J, Mumby M, Walter G.** Molecular model of the A subunit
1408 of protein phosphatase 2A interaction with other subunits and tumor antigens.
1409 Journal of Virology. 1994:**68**(1):123-129. https://doi.org/10.1128/JVI.68.1.123-
1410 129.1994
1411 **Schaart JG, Dubos C, De La Fuente IR, van Houwelingen AMML, de Vos RCH,**
1412 **Jonker HH, Xu WJ, Routaboul JM, Lepiniec L, Bovy AG.** Identification and
1413 characterization of MYB‐bHLH‐WD40 regulatory complexes controlling
1414 proanthocyanidin biosynthesis in strawberry (*Fragaria* × *ananassa*) fruits. New
1415 Phytologist. 2012:**197**(2):454-467. https://doi.org/10.1111/nph.12017
1416 **Serobatse KRN, Kabanda MM.** An appraisal of the hydrogen atom transfer mechanism
1417 for the reaction between thiourea derivatives and ·OH radical: A case-study of
1418 dimethylthiourea and diethylthiourea. Computational and Theoretical Chemistry.
1419 2017:**1101**:83-95. https://doi.org/10.1016/j.comptc.2016.12.027
1420 **Shan X, Zhang Y, Peng W, Wang Z, Xie D.** Molecular mechanism for jasmonate-
1421 induction of anthocyanin accumulation in *Arabidopsis*. Journal of Experimental
1422 Botany. 2009:**60**(13):3849-3860. https://doi.org/10.1093/jxb/erp223
1423 **Shi H, Liu G, Wei Y, Chan Z.** The zinc-finger transcription factor ZAT6 is essential for
1424 hydrogen peroxide induction of anthocyanin synthesis in *Arabidopsis*. Plant
1425 Molecular Biology. 2018:**97**(1-2):165-176. https://doi.org/10.1007/s11103-018-
1426 0730-0
1427 **Shi W, Wang X, Liu H, Cai Z, Lu C, Chen Y.** A novel ABA-insensitive mutant in
1428 Arabidopsis reveals molecular network of ABA-induced anthocyanin accumulation
1429 and abiotic stress tolerance. Journal of Plant Physiology. 2022:**278**:153810.
1430 https://doi.org/10.1038/srep29164
1431 **Söderman E, Hjellström M, Fahleson J, Engström P.** The HD-Zip gene *ATHB6* in

1432 *Arabidopsis* is expressed in developing leaves, roots and carpels and up-regulated
1433 by water deficit conditions. Plant Molecular Biology. 1999:**40**(6):1073-1083.
1434 https://doi.org/10.1023/A:1006267013170
1435 **Söderman E, Mattsson J, Engstrom P.** The *Arabidopsis* homeobox gene *ATHB-7* is
1436 induced by water deficit and by abscisic acid. Plant Journal. 1996:**10**(2):375-381.
1437 https://doi.org/10.1046/j.1365-313x.1996.10020375.x
1438 **Steyn WJ, Wand SJE, Holcroft DM, Jacobs G.** Anthocyanins in vegetative tissues: a
1439 proposed unified function in photoprotection. New Phytologist. 2002:**155**(3):349-
1440 361. https://doi.org/10.1046/j.1469-8137.2002.00482.x
1441 **Takos AM, Jaffe FW, Jacob SR, Bogs J, Robinson SP, Walker AR.** Light-induced
1442 expression of a *MYB* gene regulates anthocyanin biosynthesis in red apples. Plant
1443 Physiology. 2006:**142**(3):1216-1232. https://doi.org/10.1104/pp.106.088104
1444 **Tao R, Yu W, Gao Y, Ni J, Yin L, Zhang X, Li H, Wang D, Bai S, Teng Y.** Light-induced
1445 Basic/Helix-Loop-Helix64 enhances anthocyanin biosynthesis and undergoes
1446 CONSTITUTIVELY PHOTOMORPHOGENIC1-mediated degradation in pear.
1447 Plant Physiology. 2020:**184**(4):1684-1701. https://doi.org/10.1104/pp.20.01188
1448 **Uhrig RG, Labandera AM, Moorhead GB.** *Arabidopsis* PPP family of serine/threonine
1449 protein phosphatases: many targets but few engines. Trends in Plant Science.
1450 2013:**18**(9):505-513. https://doi.org/10.1016/j.tplants.2013.05.004
1451 **Walter M, Chaban C, Schutze K, Batistic O, Weckermann K, Nake C, Blazevic D,**
1452 **Grefen C, Schumacher K, Oecking C, et al.** Visualization of protein interactions
1453 in living plant cells using bimolecular fluorescence complementation. Plant Journal.
1454 2004:**40**(3):428-438. https://doi.org/10.1111/j.1365-313X.2004.02219.x
1455 **Wang L, Leister D, Guan L, Zheng Y, Schneider K, Lehmann M, Apel K, Kleine T.**
1456 The *Arabidopsis* SAFEGUARD1 suppresses singlet oxygen-induced stress
1457 responses by protecting grana margins. Proceedings of the National Academy of
1458 Sciences of the United States of America. 2020:**117**(12):6918-6927.
1459 https://doi.org/10.1073/pnas.1918640117
1460 **Wu Q, Su N, Zhang X, Liu Y, Cui J, Liang Y.** Hydrogen peroxide, nitric oxide and UV
1461 RESISTANCE LOCUS8 interact to mediate UV-B-induced anthocyanin

1462 biosynthesis in radish sprouts. Scientific Reports. 2016:**6**:29164.
1463 https://doi.org/10.1038/srep29164
1464 **Xie XB, Li S, Zhang RF, Zhao J, Chen YC, Zhao Q, Yao YX, You CX, Zhang XS, Hao**
1465 **YJ.** The bHLH transcription factor MdbHLH3 promotes anthocyanin accumulation
1466 and fruit colouration in response to low temperature in apples. Plant Cell and
1467 Environment. 2012:**35**(11):1884-1897. https://doi.org/10.1111/j.1365-
1468 3040.2012.02523.x
1469 **Xiong H, Hua L, Reyna-Llorens I, Shi Y, Chen KM, Smirnoff N, Kromdijk J, Hibberd**
1470 **JM.** Photosynthesis-independent production of reactive oxygen species in the rice
1471 bundle sheath during high light is mediated by NADPH oxidase. Proceedings of
1472 the National Academy of Sciences of the United States of America. 2021:**118**(25).
1473 https://doi.org/10.1073/pnas.2022702118
1474 **Xu H, Zou Q, Yang G, Jiang S, Fang H, Wang Y, Zhang J, Zhang Z, Wang N, Chen**
1475 **X.** MdMYB6 regulates anthocyanin formation in apple both through direct
1476 inhibition of the biosynthesis pathway and through substrate removal. Horticulture
1477 Research. 2020:**7**(1):72. https://doi.org/10.1038/s41438-020-0294-4
1478 **Xu W, Dubos C, Lepiniec L.** Transcriptional control of flavonoid biosynthesis by MYB-
1479 bHLH-WDR complexes. Trends in Plant Science. 2015:**20**(3):176-185.
1480 https://doi.org/10.1016/j.tplants.2014.12.001
1481 **Xu Z, Mahmood K, Rothstein SJ.** ROS induces anthocyanin production via late
1482 biosynthetic genes and anthocyanin deficiency confers the hypersensitivity to ROS-
1483 generating stresses in Arabidopsis. Plant and Cell Physiology. 2017:**58**(8):1364-
1484 1377. https://doi.org/10.1093/pcp/pcx073
1485 **Yang Q, Niu Q, Li J, Zheng X, Ma Y, Bai S, Teng Y.** PpHB22, a member of HD-Zip
1486 proteins, activates *PpDAM1* to regulate bud dormancy transition in 'Suli' pear
1487 (*Pyrus pyrifolia* White Pear Group). Plant Physiology and Biochemistry.
1488 2018:**127**:355-365. https://doi.org/10.1016/j.plaphy.2018.04.002
1489 **Yao G, Ming M, Allan AC, Gu C, Li L, Wu X, Wang R, Chang Y, Qi K, Zhang S, et**
1490 **al.** Map-based cloning of the pear gene *MYB114* identifies an interaction with other
1491 transcription factors to coordinately regulate fruit anthocyanin biosynthesis. Plant

1492 Journal. 2017:**92**(3):437-451. https://doi.org/10.1111/tpj.13666
1493 **Zhang D, Yu B, Bai J, Qian M, Shu Q, Su J, Teng Y.** Effects of high temperatures on
1494 UV-B/visible irradiation induced postharvest anthocyanin accumulation in
1495 'Yunhongli No. 1' (*Pyrus pyrifolia* Nakai) pears. Scientia Horticulturae.
1496 2012:**134**:53-59. https://doi.org/10.1016/j.scienta.2011.10.025
1497 **Zhang L, Tao R, Wang S, Gao Y, Wang L, Yang S, Zhang X, Yu W, Wu X, Li K, et al.**
1498 PpZAT5 suppresses the expression of a B-box gene *PpBBX18* to inhibit
1499 anthocyanin biosynthesis in the fruit peel of red pear. Frontiers in Plant Science.
1500 2022:**13**:1022034. https://doi.org/10.3389/fpls.2022.1022034
1501 **Zhou HW, Nussbaumer C, Chao Y, DeLong A.** Disparate roles for the regulatory A
1502 subunit isoforms in Arabidopsis protein phosphatase 2A. Plant Cell.
1503 2004:**16**(3):709-722. https://doi.org/10.1105/tpc.018994

1504

1505

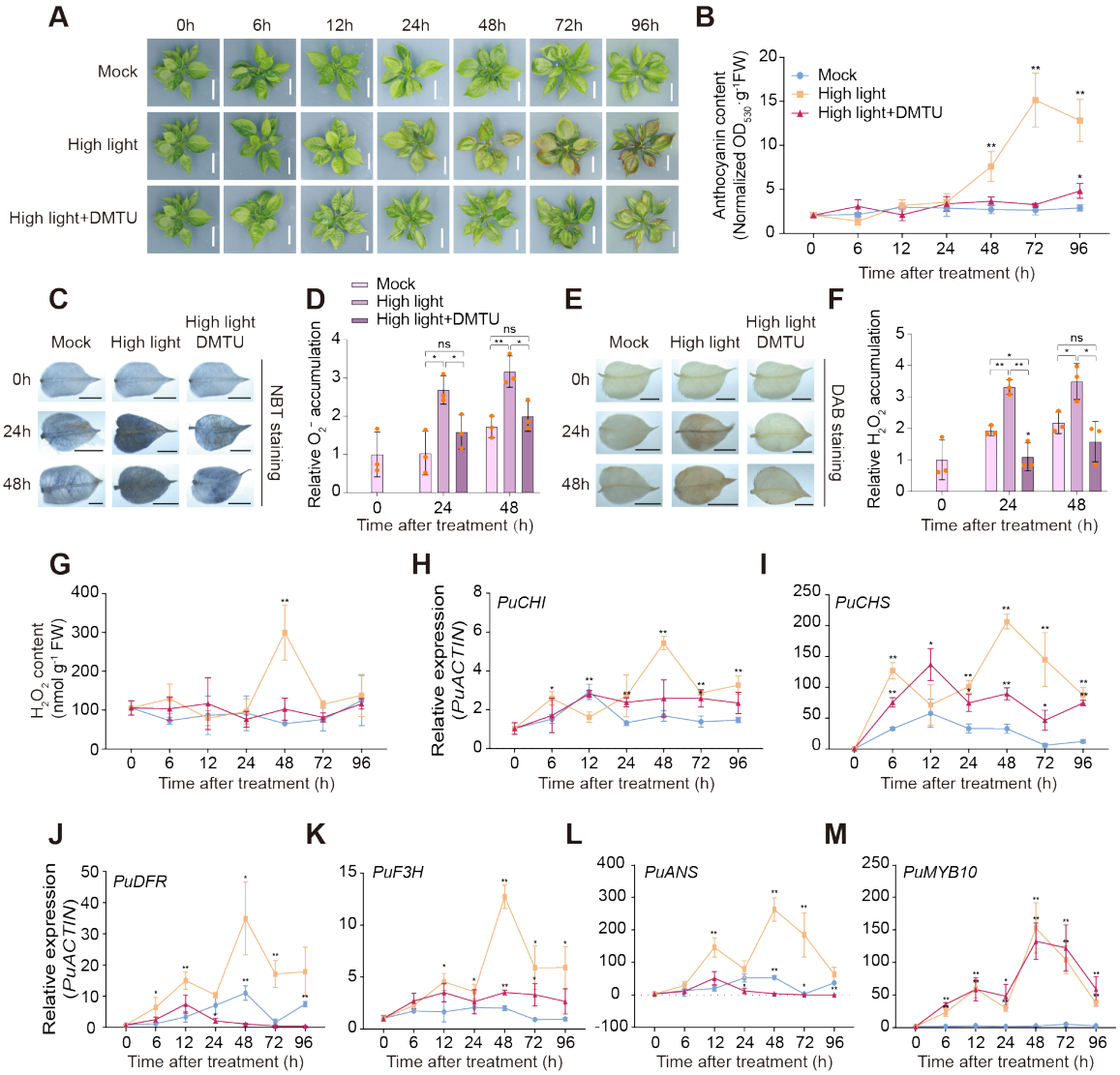

Figure 1. High-light stress-induced anthocyanin biosynthesis is ROS-dependent. (A-M), Pear seedlings were treated with high-light (photon flux density: approximately 160 μmol·s^{-1}·m^{-2}) or high-light supplemented with N, N'-dimethylthiourea (DMTU) treatment. DMTU was applied as ROS scavenger, and pear seedlings under normal light condition were used as Mock (photon flux density: approximately 50 μmol·s^{-1}·m^{-2}). Pear seedlings were sampled at 0 h, 6 h, 12 h, 24 h, 48 h, 72 h, 96 h. **(A)** Phenotype of pear seedlings (scale bar, 1 cm). **(B)** The anthocyanin contents for pear seedlings (units: A_{530}/g of fresh weight). **(C)** NBT staining for O_2^- in pear seedlings leaves at 0 h, 24 h, 48 h (scale bar, 5 mm). **(D)** Quantification of NBT staining in pear leaves at 0 h, 24 h, 48 h. **(E)** DAB staining for H_2O_2 in pear seedlings leaves at 0 h, 24 h, 48 h (scale bar, 5 mm). **(F)** Quantification of

DAB staining in pear leaves at 0 h, 24 h, 48 h. **(G)** The H_2O_2 content for pear seedlings. **(H-M),** The expression levels of *PuCHI*, *PuCHS*, *PuDFR*, *PuF3H*, *PuANS*, *PuMYB10* in pear seedlings under different treatments. *PuACTIN* was amplified as an internal control. Data are presented as means ± s.d. of 3 biological replicates. Asterisks indicate significant differences compared with Mock group **(B)** and **(G-M)**, Mock and High light stress **(D)** and **(F)** (two-tailed Student's *t-test*, $*P < 0.05$, $**P < 0.01$; ns, no significance, $P > 0.05$), all P values are shown in Supplemental Data Set S7.

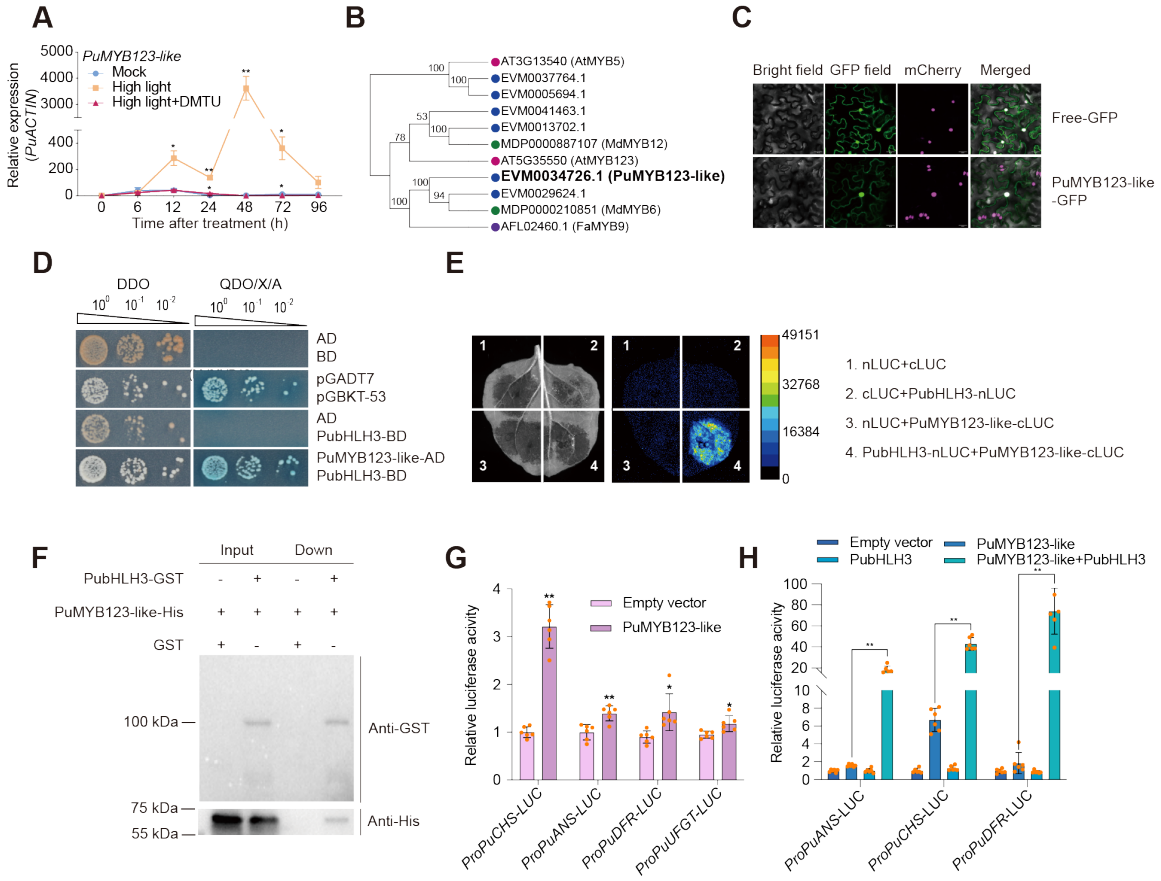

Figure 2. Identification of PuMYB123-like and its interaction with PubHLH3. (A) The expression levels of *PuMYB123-like* in pear seedlings under high-light treatment or high-light supplemented with DMTU treatment. The pear seedlings under normal light condition were used as Mock. *PuACTIN* was amplified as an internal control. **(B)** Phylogenetic analysis of PuMYB123-like. The phylogenetic tree was calculated using the maximum-likelihood method of MEGA X (version 10.1.8). Bootstrap values of 1000 replicates for each branch are shown. The protein sequences from pear (Pu, *Pyrus ussuriensis*, highlighted with blue dots), apple (Md, *Malus* × *domestica*, highlighted with green dots), Arabidopsis (At, *Arabidopsis thaliana*, highlighted with rose red dots) and strawberry (Fa, *Fragaria* × *ananassa*, highlighted with purple dots). PuMYB123-like (EVM0034726.1) is bolded and enlarged. **(C)** Subcellular localization of PuMYB123-like in *N. benthamiana* leaf cells (scale bar, 25 μm). **(D)** Interaction between PuMYB123-like and PubHLH3 in a yeast two-hybrid assay, with pGADT7-T and pGBKT7-53 as positive controls. DDO, SD/-Trp/-Leu medium; QDO/X/A, SD/-Trp/-Leu/-Ade/-His medium with X-α-gal and

Aureobasidin. **(E)** The interaction between PuMYB123-like and PubHLH3 was detected by luciferase complementation imaging assays. The pseudocolour scale bar indicates the range of luminescence intensity. **(F)** The interaction between PuMYB123-like and PubHLH3 analyzed using a pull-down assay. PuMYB123-like-His was incubated with GST or PubHLH3-GST. The interaction proteins were precipitated by GST-Trap agarose beads and analyzed by immunoblotting with an anti-GST or anti-His antibody. **(G)** A dual-luciferase assay demonstrated that PuMYB123-like promotes the promoter activity of anthocyanin-related genes (*PuCHS*, *PuANS*, *PuDFR*, *PuUFGT*). The promoter of anthocyanin-related genes was cloned into the pGreenII 0800-LUC (firefly luciferase) vector, and the full-length CDS of *PuMYB123-like* was cloned into the pGreenII 0029 62-SK vector. The empty vector of pGreenII 0029 62-SK was used as control. **(H)** Dual-luciferase assay showed that interaction between PuMYB123-like and PubHLH3 significantly enhanced activation of PuMYB123-like on *PuCHS*, *PuDFR* and *PuANS* promoters. Data are presented as means ± s.d. of 3 biological replicates **(A)** or 6 biological replicates **(G)** and **(H)**. Asterisks indicate significant differences compared with Mock **(A)**, empty vector **(G)** or PuMYB123-like **(H)** (two-tailed Student's *t-test*, $*P < 0.05$, $**P < 0.01$), all *P* values are shown in Supplemental Data Set S7.

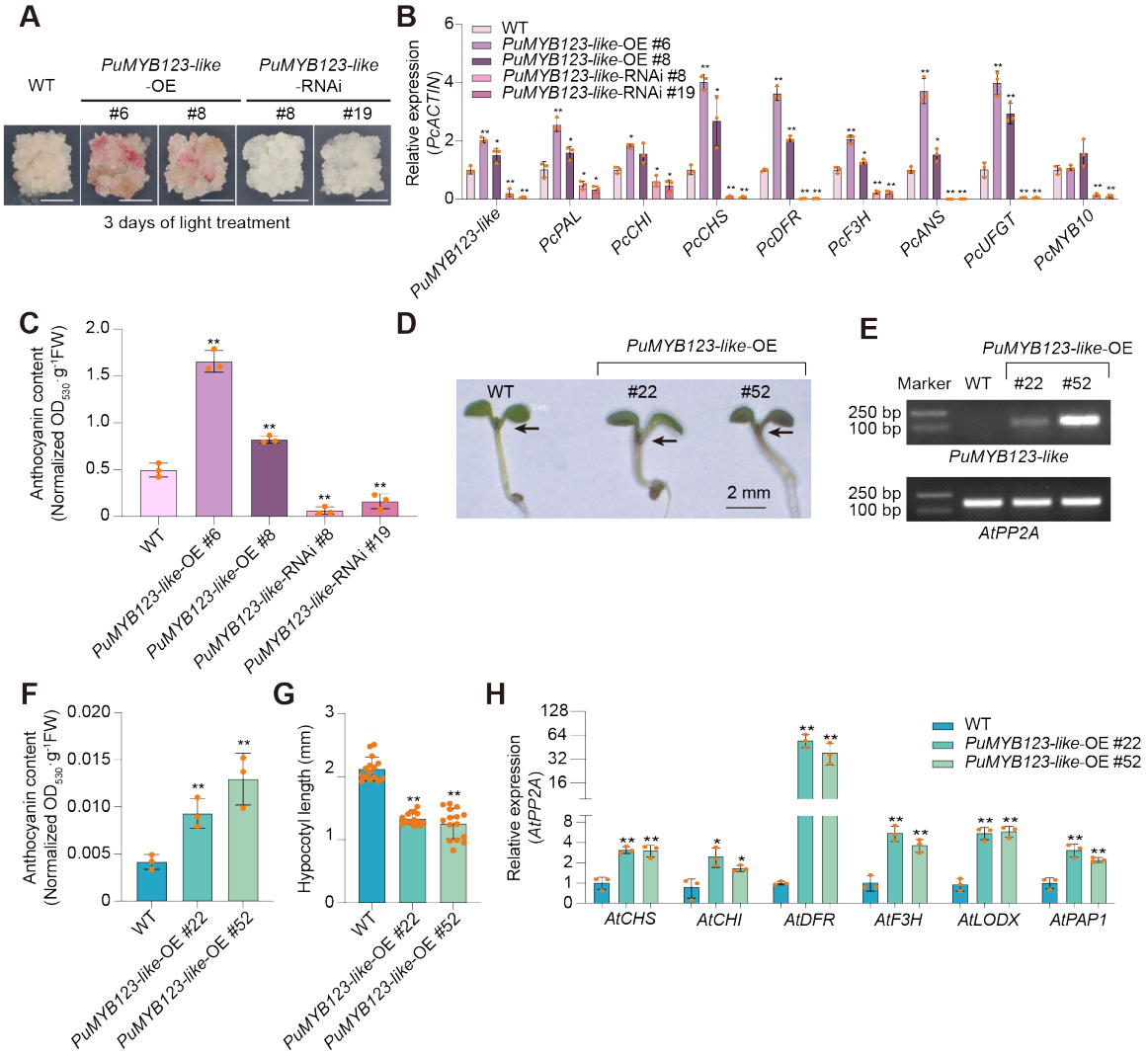

Figure 3. PuMYB123-like promotes anthocyanin biosynthesis. (A) Phenotype of pear calli overexpressing or silencing *PuMYB123-like* (scale bar, 1 cm). Wild type pear calli were used as the negative control. Pear calli were incubated under continuous white light at 17°C for 3 d. **(B)** Expression levels of anthocyanin-related genes and *PuMYB123-like* in *PuMYB123-like*-OE *and PuMYB123-like*-RNAi pear calli after light treatment. *PcACTIN* was amplified as an internal control. **(C)** Anthocyanin contents in *PuMYB123-like*-OE and *PuMYB123-like*-RNAi pear calli after light treatment (units: A_{530}/g of fresh weight). **(D)** Phenotype of *Arabidopsis* seedlings ectopic expressing *PuMYB123-like* (scale bar, 2 mm). Wild-type *Col 0* was used as the negative control. *Arabidopsis* seedlings were grown on 1/2 MS medium for five days. **(E)** PCR pattern of wild-type pear calli and *PuMYB123-like* transgenic pear calli lines using transgene-specific primers. *AtPP2A* was amplified as an

internal control. **(F)** Anthocyanin contents in transgenic *Arabidopsis* lines (units: A_{530}/g of fresh weight). **(G)** The hypocotyl length of transgenic *Arabidopsis* seedlings. **(H)** Expression levels of anthocyanin-related genes in transgenic *Arabidopsis* lines. Data are presented as means ± s.d. of 3 biological replicates **(B)**, **(C)**, **(F)** and **(H)** and 15 biological replicates **(G)**. Asterisks indicate significant differences compared with wild type pear calli **(B)** and **(C)** or wild type *Arabidopsis* **(F-H)**, (two-tailed Student's *t-test*, $*P < 0.05$, $**P < 0.01$), all *P* values are shown in Supplemental Data Set S7.

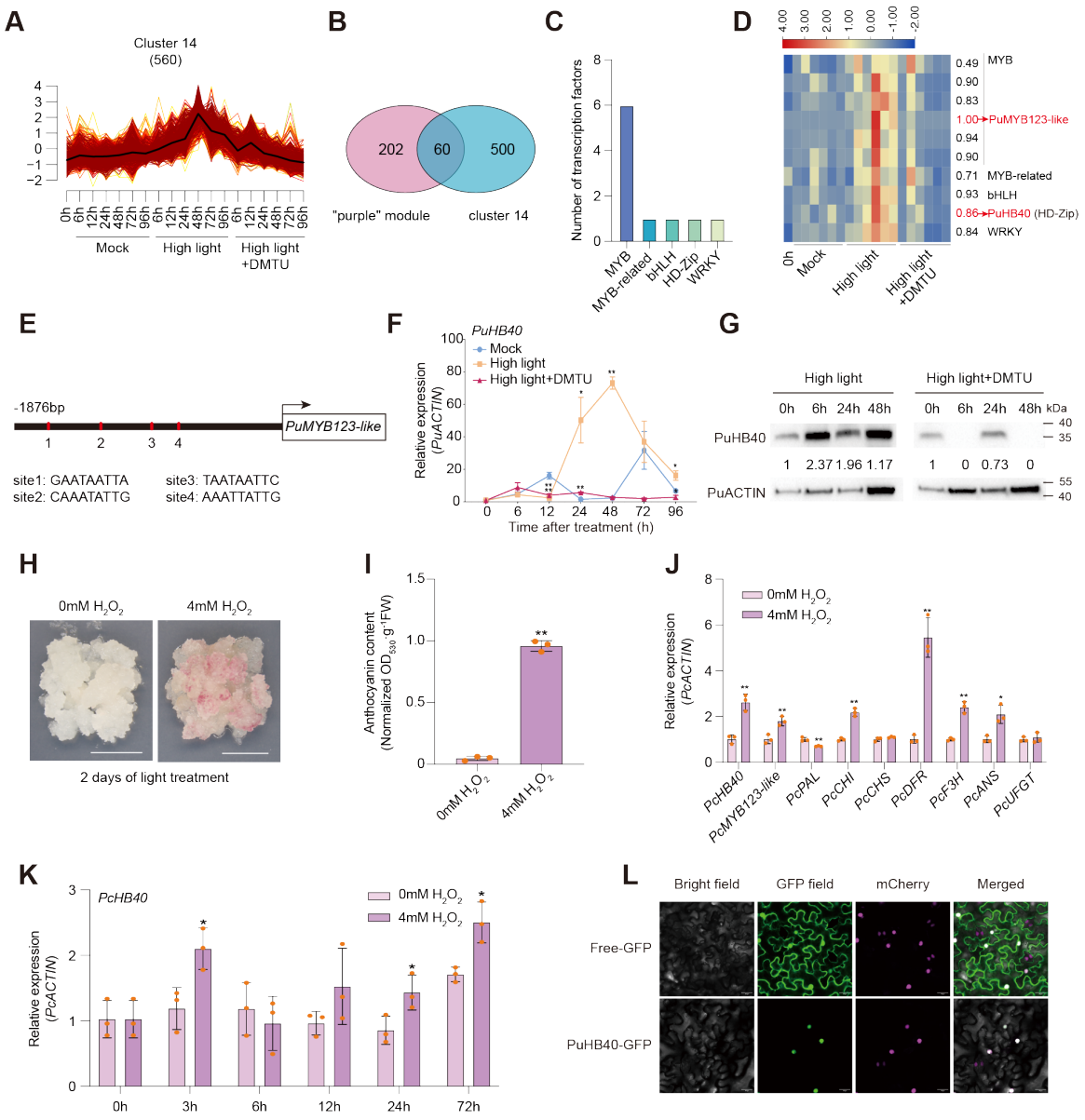

Figure 4. Identification of PuHB40 and its response to ROS. **(A)** The expression pattern of DETs in cluster 14 based on Mfuzz clustering. **(B)** Venn diagram of genes in "purple module" and DETs in cluster 14. **(C)** Numbers of transcription factors in overlapped genes of "purple module" and cluster 14. **(D)** Heat map presenting the expression patterns of transcription factors in overlapped genes of "purple module" and cluster 14 in response to diverse treatments. The values on the right of the heat map indicate the correlation of the expression patterns (FPKMs) between these genes and *PuMYB123-like*. **(E)** Distribution of potential binding sites of PuHB40 in *PuMYB123-like* promoter region. Vertical red lines indicate the position of site1 to site4. **(F)** The expression levels of *PuHB40* in pear seedlings

under high-light treatment or high-light supplemented with DMTU treatment, and pear seedlings under normal light condition were used as Mock. *PuACTIN* was amplified as an internal control. **(G)** Changes in the PuHB40 abundance in pear seedlings under high-light treatment or high-light supplemented with DMTU treatment for 0 h, 6 h, 24 h, 48 h. The PuHB40 and PuACTIN proteins were detected by immunoblotting with an affinity-purified specific anti-PuHB40 polyclonal antibody and Anti β-Actin monoclonal antibody, respectively. **(H)** Phenotype of pear calli after 4 mM H_2O_2 treatment for two days (scale bar, 1 cm). Pear calli treated with 0 mM H_2O_2 were used as control. **(I)** Anthocyanin contents in pear calli treated with 0 mM or 4 mM H_2O_2 for two days (units: A_{530}/g of fresh weight). **(J)** Expression levels of *PcHB40*, *PcMYB123-like* and anthocyanin-related genes in pear calli treated with 0 mM or 4 mM H_2O_2 for two days. *PcACTIN* was amplified as an internal control. **(K)** Expression levels of *PcHB40* in pear calli after 0 mM or 4 mM H_2O_2 treatment at 0 h, 3 h, 6 h, 12 h, 24 h, 72 h. *PcACTIN* was amplified as an internal control. **(L)** Subcellular localization of PuHB40 in *N. benthamiana* leaf cells (scale bar, 25 μm). Data are presented as means ± s.d. of 3 biological replicates. Asterisks indicate significant differences compared with Mock **(F)** or 0 mM H_2O_2 **(I-K)** (two-tailed Student's *t-test*, $*P < 0.05$, $**P < 0.01$), all *P* values are shown in Supplemental Data Set S7.

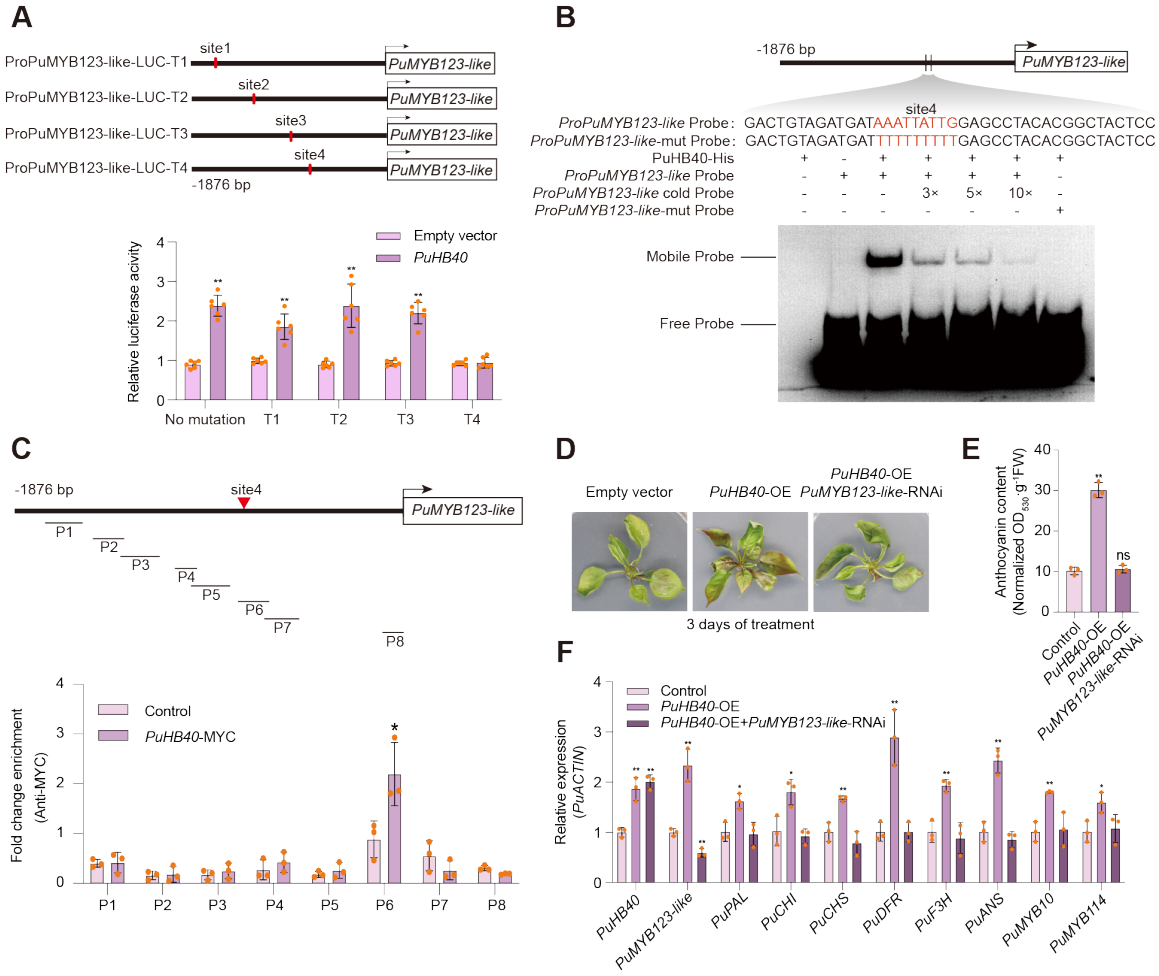

Figure 5. PuHB40 promotes *PuMYB123-like* transcription. (A) Effect of the mutation of potential PuHB40 binding sites on the activation of *PuMYB123-like*. Four potential binding sites (site1 to site4) were mutated into TTTTTTTTT, respectively. The promoters of *PuMYB123-like* with or without potential binding site mutation were cloned into the pGreenII 0800-LUC (firefly luciferase) vector, and the full-length CDS of *PuHB40* was cloned into the pGreenII 0029 62-SK vector. The empty vector of pGreenII 0029 62-SK was used as control. **(B)** The EMSA confirmed that PuHB40 bound to the site4 in the *PuMYB123-like* promoter directly. The *ProPuMYB123-like* probe was the biotin-labeled fragment of *PuMYB123-like* promoter containing site4 (AAATTATTG), whereas the cold probe was an unlabeled probe (3-, 5-, and 10-fold molar excess). *ProPuMYB123-like*-mut probe was the same as the *ProPuMYB123-like* probe but with site4 (AAATTATTG) mutated to TTTTTTTTT. **(C)** ChIP-qPCR assay results showed the binding of PuHB40 to the *PuMYB123-like* promoter *in vivo*. Cross-linked chromatin samples were extracted from

PuHB40-MYC overexpressing pear calli with 3 biological replicates and precipitated with an anti-MYC antibody. Eluted DNA was used to amplify *PuMYB123-like* promoter fragments and eight regions (P1 to P8) were examined, among which P6 containing site4. Pear calli overexpressing the *MYC* sequence were used as a negative control. Three biological replicates of pear calli were used in the ChIP assay. **(D)** Transient overexpression of *PuHB40* with or without transient silencing of *PuMYB123-like* in pear seedlings. The full-length CDS of *PuHB40* and reverse complementary gene fragment (~200 to 300 bp) of *PuMYB123-like* were inserted into the pCAMBIA1301 vector under the control of the 35S promoter. The plasmids were transformed into *A. tumefaciens* GV3101 and infiltrated into pear seedlings by vacuum. The infiltrated pear seedlings were firstly incubated in darkness for two days and then exposed to continuous white light for three days. Pear seedlings infiltrated with an empty pCAMBIA1301 vector were used as a control. **(E)** Anthocyanin contents in pear seedlings (units: A_{530}/g of fresh weight). **(F)** Expression levels of *PuHB40*, *PuMYB123-like* and anthocyanin-related genes in pear seedlings. Data are presented as means ± s.d. of 3 biological replicates **(C), (E)** and **(F)** or 6 biological replicates **(A)**. Asterisks indicate significant differences compared with empty vector **(A)** or control **(C), (E)** and **(F)** (two-tailed Student's *t-test*, $*P < 0.05$, $**P < 0.01$; ns, no significance, $P > 0.05$), all *P* values are shown in Supplemental Data Set S7.

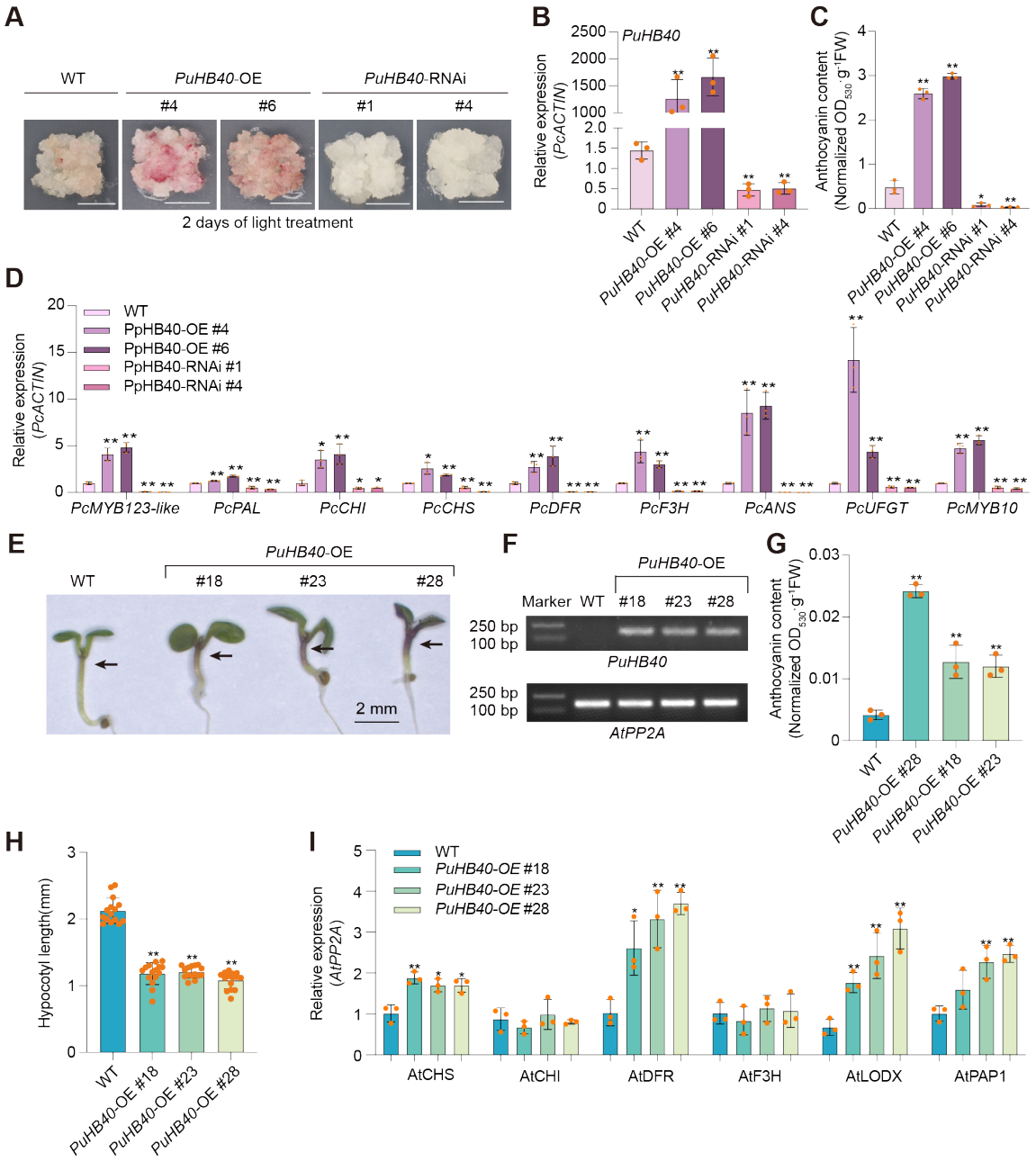

Figure 6. PuHB40 promotes anthocyanin biosynthesis. (A) Phenotype of pear calli overexpressing and silencing *PuHB40* (scale bar, 1 cm). Wild type pear calli were used as the negative control. Pear calli were incubated under continuous white light at 17°C for 3 d. **(B)** Expression levels of *PuHB40* in *PuHB40*-OE and *PuHB40*-RNAi pear calli after light treatment. *PcACTIN* was amplified as an internal control. **(C)** Anthocyanin contents in *PuHB40*-OE and *PuHB40*-RNAi pear calli after light treatment (units: A_{530}/g of fresh weight). **(D)** Expression levels of *PcMYB123-like* and anthocyanin-related genes in

PuHB40-OE and *PuHB40*-RNAi pear calli after light treatment. *PcACTIN* was amplified as an internal control. **(E)** Phenotype of *Arabidopsis* seedlings ectopic expressing *PuHB40* (scale bar, 2 mm). Wild-type *Arabidopsis* Col-0 was used as the negative control. *Arabidopsis* seedlings were grown on 1/2 MS medium for five days. **(F)** PCR results of wild-type pear calli and *PuHB40* transgenic pear calli lines using transgene-specific primers. *AtPP2A* was amplified as an internal control. **(G)** Anthocyanin contents in transgenic *Arabidopsis* lines (units: A_{530}/g of fresh weight). **(H)** The hypocotyl lengths of transgenic *Arabidopsis* seedlings (units: A_{530}/g of fresh weight). **(I)** Expression levels of anthocyanin-related genes in transgenic *Arabidopsis* lines. Data are presented as means ± s.d. of 3 biological replicates **(B-D)**, **(G)** and **(I)** or 15 biological replicates **(H)**. Asterisks indicate significant differences compared with wild type pear calli **(B-D)** or wild type *Arabidopsis* **(G-I)** (two-tailed Student's *t-test*, $*P < 0.05$, $**P < 0.01$), all P values are shown in Supplemental Data Set S7.

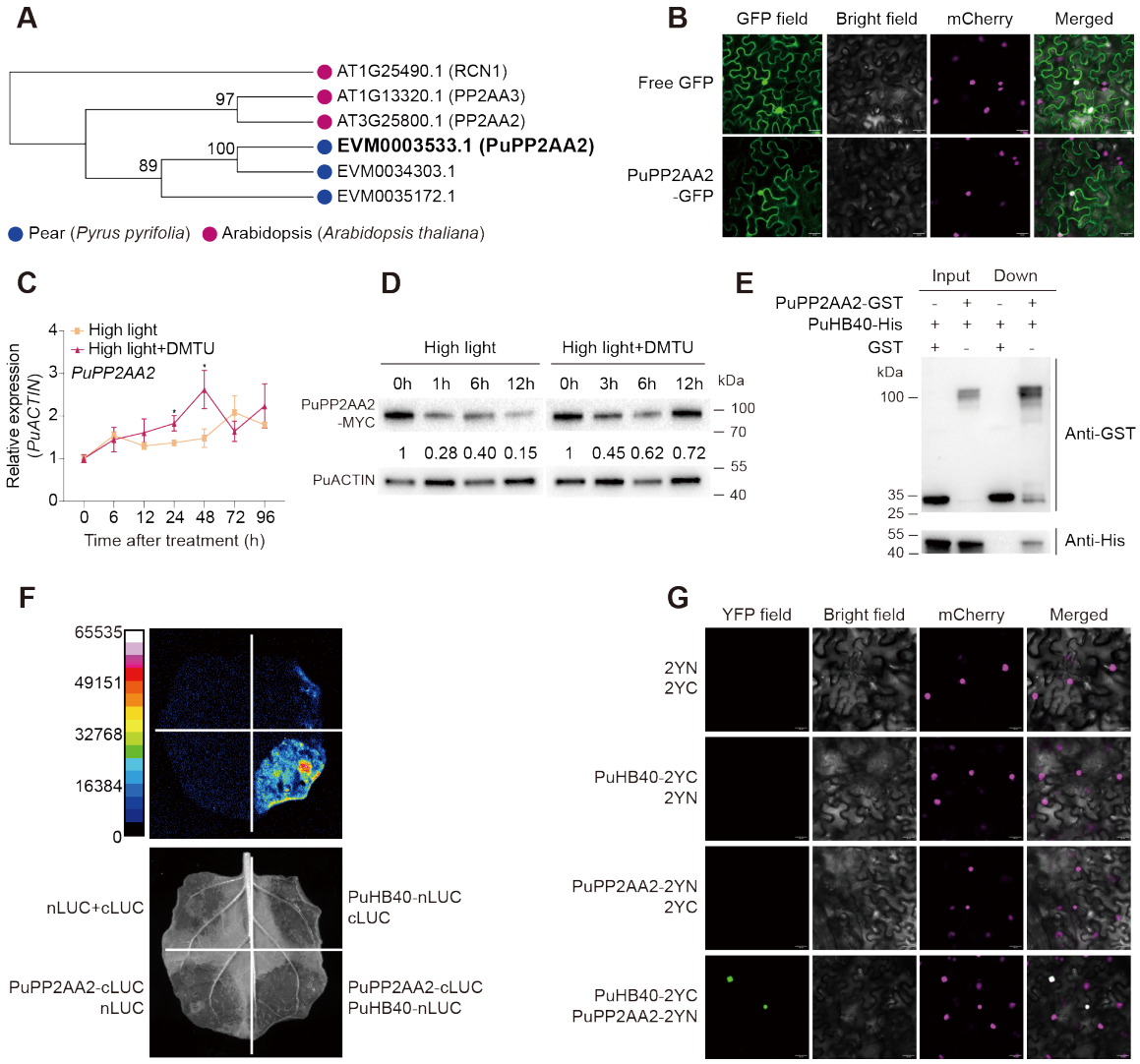

Figure 7. Identification of PuPP2AA2 and its interaction with PuHB40. (A) Phylogenetic analysis of PuPP2AA2. The phylogenetic tree was calculated using the maximum-likelihood method of MEGA X (version 10.1.8). Bootstrap values of 1000 replicates for each branch are shown. The protein sequences from pear (Pu, *Pyrus ussuriensis*, highlighted with blue dots) and Arabidopsis (*Arabidopsis thaliana*, highlighted with rose red dots). PuPP2AA2 (EVM0003533.1) is bolded and enlarged. **(B)** Subcellular localization of PuPP2AA2 in *N. benthamiana* leaf cells (scale bar, 25 μm). **(C)** The expression levels of *PuPP2AA2* in pear seedlings under high-light treatment or high-light supplemented with DMTU treatment. *PuACTIN* was amplified as an internal control. **(D)** Changes in the PuPP2AA2 abundance in pear seedlings. Pear seedlings with the transient

overexpression of MYC-tagged *PuPP2AA2* were exposed to high-light treatment or high-light supplemented with DMTU treatment for 0 h, 3 h, 6 h, 12 h. The PuPP2AA2 and PuACTIN proteins were detected by immunoblotting with anti-MYC monoclonal antibody and Anti β-Actin monoclonal antibody, respectively. **(E)** The interaction between PuPP2AA2 and PuHB40 using the pull-down assay. PuHB40-His was incubated with GST or PuPP2AA2-GST. The interactive proteins were precipitated by GST-Trap agarose beads and analyzed by immunoblotting with an anti-GST or anti-His antibody. **(F)** The interaction between PuPP2AA2 and PuHB40 was detected by luciferase complementation imaging assays. The pseudocolour scale bar indicates the range of luminescence intensity. **(G)** Physical association between PuPP2AA2 and PuHB40 confirmed by a BiFC assay. Fluorescence indicates positive interactions (scale bar, 25 μm). Data are presented as means ± s.d. of 3 biological replicates. Asterisks indicate significant differences compared with high-light stress supplemented with DMTU treatment (two-tailed Student's *t-test*, $*P < 0.05$), all P values are shown in Supplemental Data Set S7.

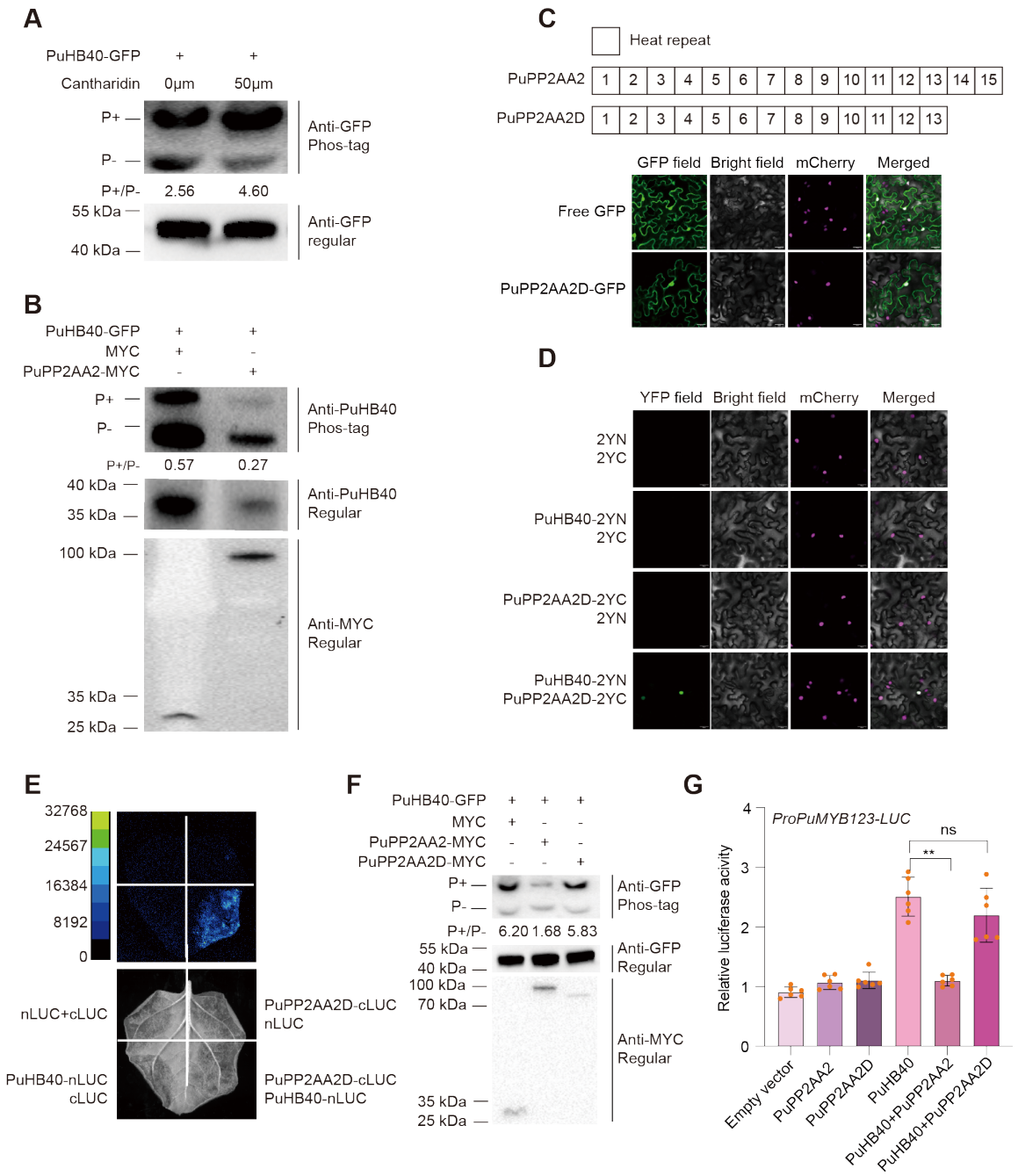

Figure 8. PuHB40 was dephosphorylated by PP2A phosphatase. (A) Phos-tag analysis of phosphorylation of PuHB40 after cantharidin treatment. *A. tumefaciens* GV3101 containing PuHB40-GFP plasmid was infiltrated into *N. benthamiana* leaves by injection and 50 μM cantharidin was injected into the same position as the agrobacteria after 24 h. *N. benthamiana* leaves injected with DMSO of corresponding concentration were used as negative control. Protein samples were extracted from *N. benthamiana* leaves after 24 h

and were separated in a Phos-tag gel (upper panel), and PuHB40-GFP with different phosphorylated status was detected using the anti-GFP antibody. Total PuHB40-GFP proteins were also analyzed by SDS-PAGE without Phos-tag (indicated as "Regular"), and were detected using anti-GFP antibody (lower panel). P+ and P- indicate phosphorylated and non-phosphorylated form of PuHB40, respectively. The intensity of the bands was measured with the Image J software and the ratio of P+/P− bands was calculated. **(B)** Immunoblotting analysis showing that the PP2A complex directly dephosphorylates PuHB40 *in vitro*. MYC, PP2A complex, and PuHB40-GFP were immunopurified from pear seedlings transiently overexpressing MYC, PuPP2AA2-MYC, and PuHB40-GFP using MYC-Trap or GFP-Trap, respectively. After incubation of PP2A complexes with PuHB40-GFP (MYC with PuHB40-GFP was set as control), protein samples in the reaction system were separated in Phos-tag gel (upper panel) and detected using the anti-PuHB40 antibody. The intensity of the bands was measured with the Image J software and the ratio of P+/P− bands was calculated Total proteins in the reaction system were analyzed by SDS-PAGE without Phos-tag (indicated as "Regular"). PuHB40-GFP, MYC and PuPP2AA2-MYC were set as the loading controls and detected by the anti-PuHB40 (middle panel) or anti-MYC (lower panel) antibody, respectively. **(C)** Subcellular localization of PuPP2AA2D in *N. benthamiana* leaf cells (scale bar, 25 μm). PuPP2AA2D is PuPP2AA2 with the deletion of heat repeats 14 and 15 in the C-terminal. **(D)** The interaction between PuPP2AA2D and PuHB40 confirmed by a BiFC assay. Fluorescence indicates positive interactions (scale bar, 25 μm). **(E)** The interaction between PuPP2AA2D and PuHB40 was detected by luciferase complementation imaging assays. The pseudocolour scale bar indicates the range of luminescence intensity. **(F)** Immunoblotting analysis showing that PP2A dephosphorylates PuHB40 *in vivo*. Protein extracts from *N. benthamiana* leaves co-infiltrated PuHB40-GFP with MYC, PuPP2AA2-MYC, or PuPP2AA2D-MYC were separated in Phos-tag gel (upper panel) and detected using the anti-GFP antibody (MYC with PuHB40-GFP was set as control). The intensity of the bands was measured with the Image J software and the ratio of P+/P− bands was calculated. Total PuHB40-GFP, MYC, PuPP2AA2-MYC and PuPP2AA2D-MYC proteins were also analyzed by SDS-PAGE without Phos-tag (indicated as "Regular"). PuHB40-GFP, MYC, PuPP2AA2-MYC and

PuPP2AA2D-MYC were set as the loading controls and detected by the anti-GFP (middle panel) or anti-MYC (lower panel) antibody, respectively. **(G)** Dual-luciferase assay showed that dephosphorylation of PuHB40 by PP2A significantly inhibited the activation of *PuMYB123-like* promoter by PuHB40. The *PuMYB123-like* promoter was cloned into the pGreenII 0800-LUC (firefly luciferase) vector, and the full-length CDS of *PuHB40*, *PuPP2AA2* and *PuPP2AA2D* were cloned into the pGreenII 0029 62-SK vector. The PuHB40 was used as control. Data are presented as means ± s.d. of 6 biological replicates **(G)**. Asterisks indicate significant differences compared PuHB40 **(G)** (two-tailed Student's *t-test*, $^{**}P < 0.01$; ns, no significance, $P > 0.05$), all P values are shown in Supplemental Data Set S7.

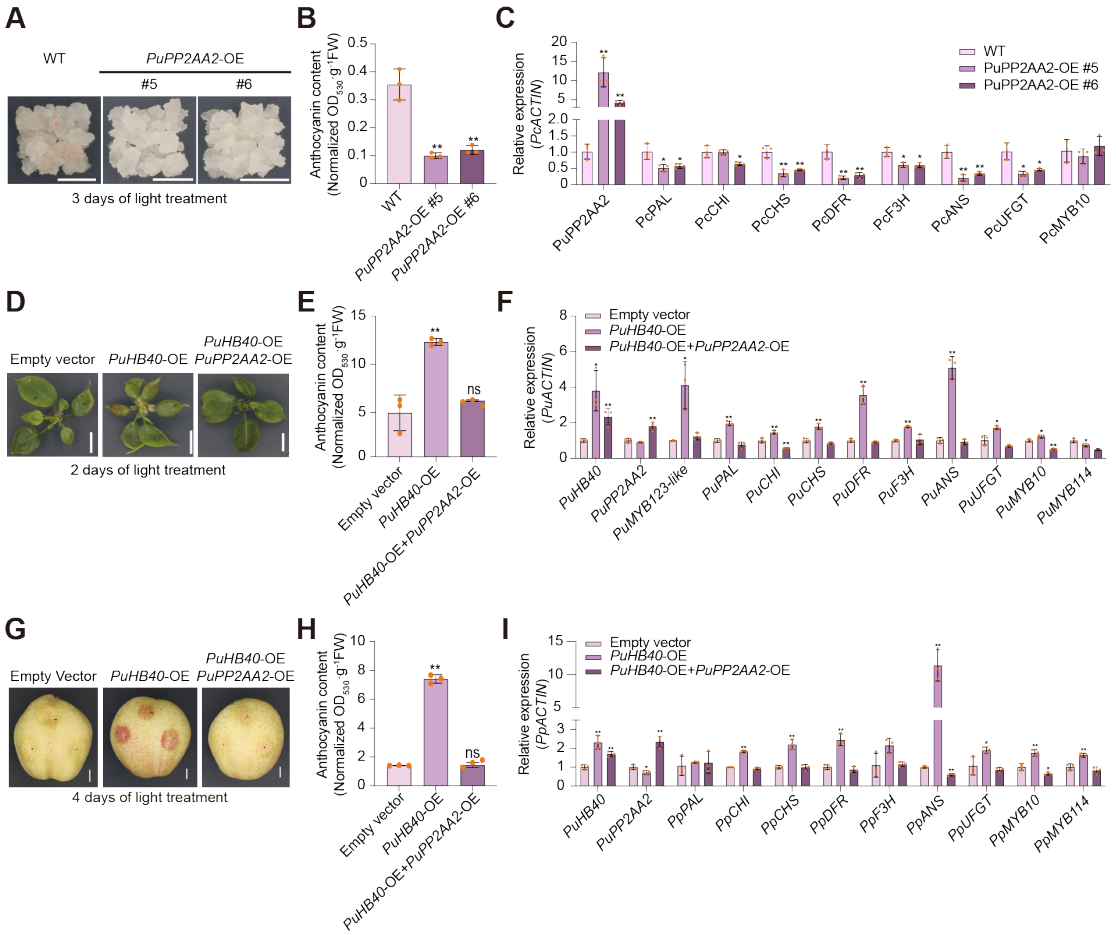

Figure 9. Attenuation of PuHB40-induced anthocyanin biosynthesis by PuPP2AA2. **(A)** Phenotype of pear calli overexpressing *PuPP2AA2* (scale bar, 1 cm). Wild type pear calli were used as the negative control. Pear calli were incubated under continuous white light at 17°C for 3 d. **(B)** Anthocyanin contents in *PuPP2AA2*-OE after light treatment (units: A_{530}/g of fresh weight). **(C)** Expression levels of *PuPP2AA2* and anthocyanin-related genes in *PuPP2AA2*-OE pear calli after light treatment. *PcACTIN* was amplified as an internal control. **(D)** Transient overexpression of *PuHB40* with or without transient overexpressing of *PuPP2AA2* in pear seedlings. The full-length CDS of *PuHB40* and *PuPP2AA2* were inserted into the pCAMBIA1301 vector under the control of the 35S promoter. The plasmids were transformed into *A. tumefaciens* GV3101 and infiltrated into pear seedlings by vacuum. The infiltrated pear seedlings were firstly incubated in darkness for two days and then exposed to continuous white light for three days. Pear seedlings infiltrated with an empty pCAMBIA1301 vector were used as a control. **(E)** Anthocyanin

contents in pear seedlings (units: A_{530}/g of fresh weight). **(F)** Expression levels of *PuHB40*, *PuPP2AA2*, *PuMYB123-like* and anthocyanin-related genes in pear seedlings. **(G)** Transient overexpression of *PuHB40* with or without transient overexpressing of *PuPP2AA2* in pear fruits (scale bar, 1 cm). The full-length CDS of *PuHB40* and *PuPP2AA2* were cloned to the pGreenII 0029 62-SK vector under the control of the 35S promoter. Pear fruits were infiltrated with *A. tumefaciens* GV3101 cells containing the recombinant plasmid using a needle syringe. Fruits infiltrated with an empty pGreenII 0029 62-SK vector were used as a control. The phenotypes were examined after dark treatment for one day followed by the light treatment for four days **(H)** Total anthocyanin contents in pear fruits (units: A_{530}/g of fresh weight). **(I)** Expression levels of *PuHB40*, *PuPP2AA2* and anthocyanin-related genes in pear fruits. Data are presented as means ± s.d. of 3 biological replicates. Asterisks indicate significant differences compared with wild type pear calli **(B)** and **(C)** or empty vector **(E), (F), (H)** and **(I)** (two-tailed Student's *t-test*, $*P < 0.05$, $**P < 0.01$; ns, no significance, $P > 0.05$), all P values are shown in Supplemental Data Set S7.

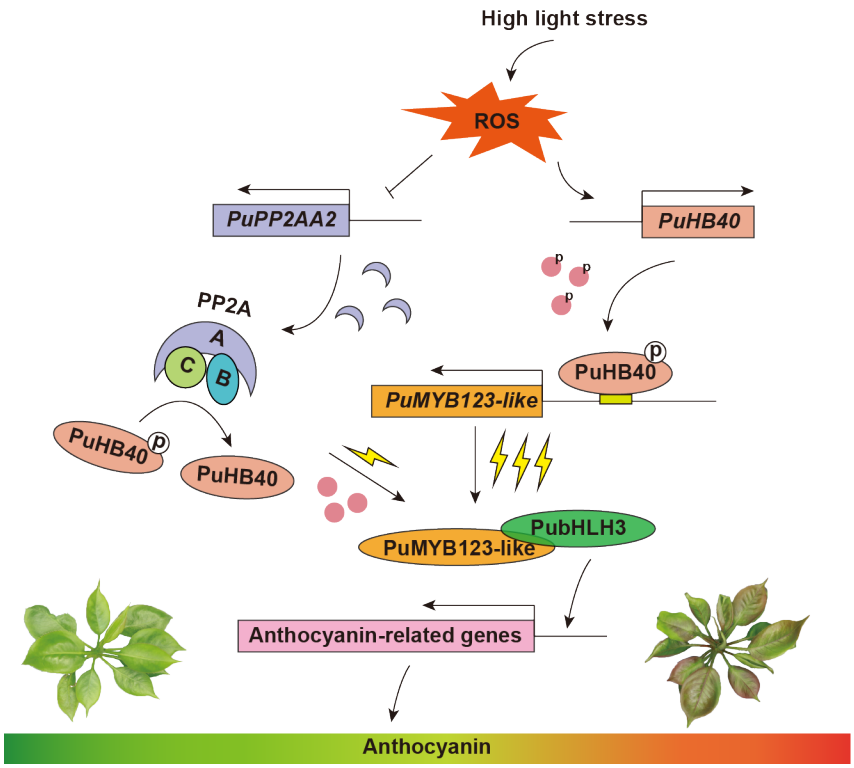

Figure 10. Proposed model for PuHB40-mediated ROS-dependent anthocyanin biosynthesis in pears. PuHB40 is the key transcription factor in ROS-induced anthocyanin biosynthesis. ROS promote PuHB40 expression and then positively regulate its transcriptional activity on PuMYB123-like/PubHLH3 complex to induce anthocyanin biosynthesis. The transcriptional activity of PuHB40 depends on its phosphorylation level which is regulated by PP2A. ROS maintain phosphorylation of PuHB40 at a high level, and enhance the transcriptional activity of PuHB40 on *PuMYB123-like* by suppressing the transcription of *PuPP2AA2* under high-light stress, and thus promote anthocyanin biosynthesis.